

Workshop and Conference on  
**EL NIÑO & TROPICAL OCEAN-ATMOSPHERE INTERACTIONS**  
(3 – 14 June 2002)

---

**"The Coupled Ocean-Atmosphere System"**

Ping CHANG  
Texas A & M University  
Dept. Physical Oceanography  
College Station, Texas  
U.S.A.

---

These are preliminary lecture notes, intended only for distribution to participants



# Coupled Mechanisms

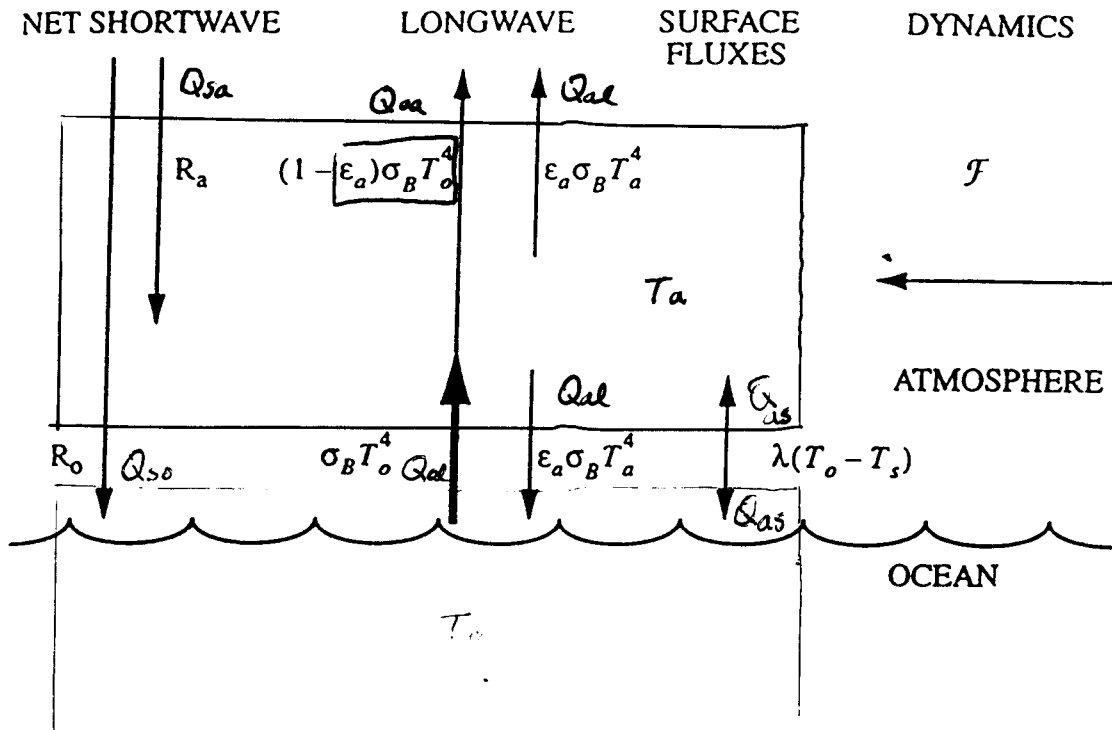
## Passive Coupling :

1. An Energy Balance Model
2. Mixed Layer Feedback, Spectrum and Predictability

## Active Coupling :

1. Dynamic Feedbacks
  - Bjerknes Mechanism
  - Ekman Mechanism
2. Thermodynamic Feedbacks
  - Wind-Evaporation-SST Feedback
  - Cloud-SST Feedback

Barsagli & Battisti (JAS, 1998)  
 Bretherton & Battisti (GRL, 1999)



Assume:  $Q_{sa} = \bar{Q}_{sa} + Q'_{sa}$ ;  $Q'_{sa} = 0$

$Q_{so} = \bar{Q}_{so} + Q'_{so}$ ;  $Q'_{so} = 0$

$Q_{ol} = \sigma_B T_o^4 \rightarrow Q_{ol} = \sigma_B (\bar{T}_o + T_o')^4 \approx \sigma_B \bar{T}_o^4 + 4\sigma_B \bar{T}_o^3 T_o'$

$Q_{oa} = \epsilon_a \sigma_B T_o^4$  :

$Q_{al} = \epsilon_a \sigma_B T_a^4$  .

$\epsilon_a$  = long wave emissivity

$\sigma_B$  = stefan-Boltzman constant

# An Energy Balance Coupled Model

## Assumptions :

1. Atmosphere: a single graybody layer with temperature  $T_a$  and heat capacity  $\gamma_a$
2. Ocean: a well-mixed layer with temperature  $T_o$  and heat capacity  $\gamma_o$

$$\gamma_a \frac{dT_a}{dt} = Q_{sa} + Q_{oa} - 2Q_{al} + Q_{as} + F, \quad (1)$$

$$\gamma_o \frac{dT_o}{dt} = Q_{so} + Q_{al} - Q_{ol} - Q_{as}, \quad (2)$$

where

- $Q_{sa}, Q_{oa}$ : Short & longw. radiation gain by atmos,
- $Q_{al}$ : Longwave radiation loss by atmos,
- $Q_{as}$ : Air-sea flux exchange,
- $F$ : Other processes,
- $Q_{so}, Q_{al}$ : Short & longw. radiation gain by ocean,
- $Q_{ol}$ : Radiation loss by ocean.

## Coupled Mixed Layer Model

**Linearization** : All the  $Q$ s are radiative fluxes proportional to  $\sigma_B T^4$ , except for  $Q_{as}$  – the combined latent and sensible fluxes, which is assumed to be proportional to air-sea temperature difference ( $T_o - T_a$ ). Linearization of these fluxes about the climatological temperature, i.e.,  $Q = dQ/dT(T - \langle T \rangle)$ , gives a coupled mixed layer model:

$$\gamma_a \frac{dT'_a}{dt} = -\lambda(T'_a - T'_o) - \lambda_a T'_a + F, \quad (3)$$

$$\gamma_o \frac{dT'_o}{dt} = \lambda(T'_a - T'_o) - \lambda_o T'_o, \quad (4)$$

where

- $T'_a, T'_o$ : Atmos. & ocean temperature anomalies,
- $\lambda_a, \lambda_o$ : Atmos. & ocean thermal damping,
- $\lambda$ : Air-sea feedback coefficient.

**Passive Coupling** :  $Q_{as} = \lambda(T'_a - T'_o)$  represents a negative feedback between the atmosphere and ocean.

## Properties of Coupled ML Model

**Mixed-Layer Damping** : Since heat capacity of the ocean  $\gamma_o$  is greater than the atmosphere  $\gamma_a$  by more than a factor of 20,  $\frac{dT'_a}{dt}$  can be set to zero.

$$\frac{dT'_o}{dt} = -\lambda_m T'_o + N, \quad T'_a = aT'_o + bN. \quad (5)$$

Damping time scale =  $\lambda_m^{-1} \propto$  mixed layer depth  $H_m$ .  
For  $H_m = 50m$ ,  $\lambda_m^{-1} \sim 3$  months.

**Spectra** : For a white noise forcing  $N$ ,  $T'_o$  spectrum is **red**.  $T'_a$  spectrum is also **red** because of the passive coupling. The coupling also enhances the variances in both the ocean and the atmosphere.

**Predictability** : The predictability of the system is given by persistence  $\exp(-\lambda_m t)$ . For a 50 m mixed layer, a small fraction of the atmospheric variability may be predictable a season in advance.

**Null Hypothesis** : The mixed layer feedback/passive coupling can be used as a null hypothesis for testing the importance of active coupling.

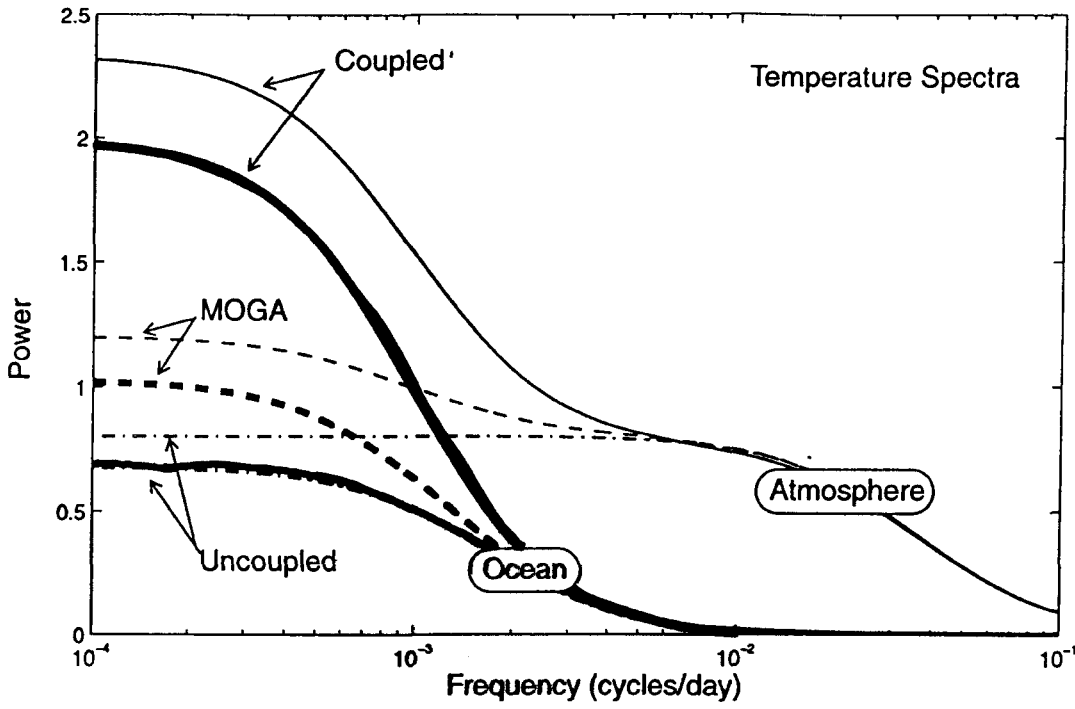


FIG. 4. Power spectra of atmosphere and ocean temperature for the coupled, MOGA, and uncoupled cases. The standard parameters (see Table 1) are used.

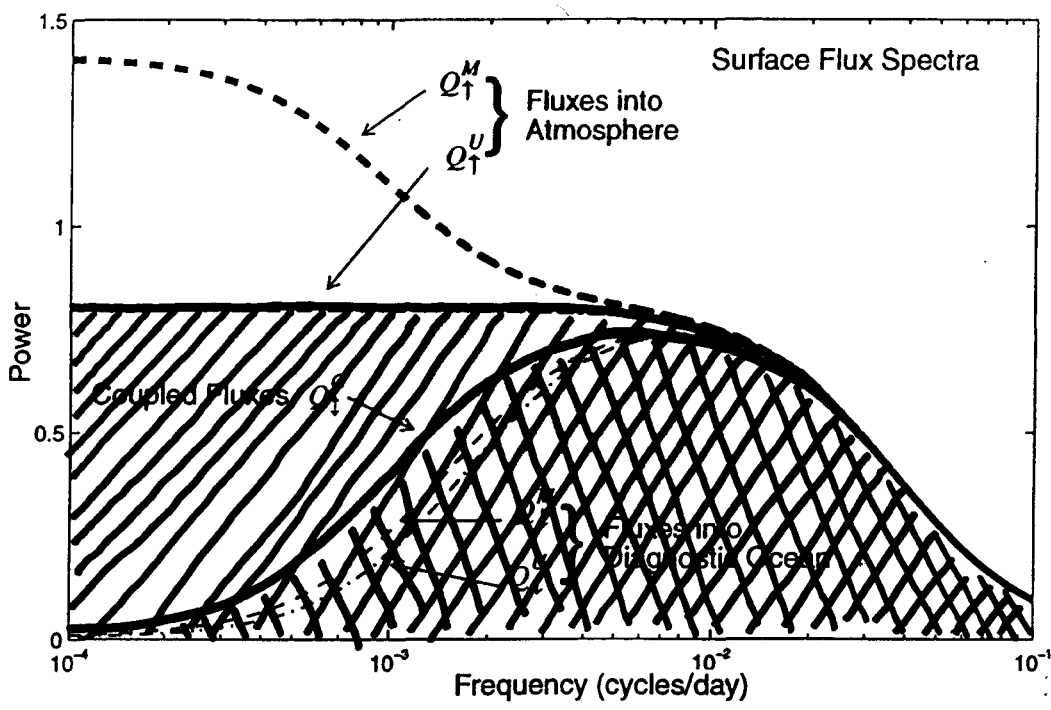


FIG. 7. Power spectra of surface flux, defined as  $Q = T_s - T_o$ , for coupled, MOGA, and uncoupled cases using the standard parameters. The fluxes into the atmosphere ( $\uparrow$ ), the fluxes into the diagnostic ocean model ( $\downarrow$ ), and the coupled fluxes ( $\updownarrow$ ) are shown. The symbols are defined in section 3c.

$$\int_0^{\infty} |Q_{\updownarrow}^c|^2 d\sigma < \int_0^{\infty} |Q_{\up}^u|^2 d\sigma$$

Bersugli and Battisti (1991)

# Active Coupling

**Break-Down of the Null-Hypothesis** : The simple coupled model based on energy balance breaks down in the tropics because a series of positive feedbacks takes effect, causing active coupling between the tropical atmosphere and oceans. The tropical atmosphere is convectively unstable, and thus highly sensitive to changes in SST. The tropical oceans have fast adjustment time scale and sensitive to changes in the winds. Therefore, the feedback between the winds and SST is the center piece of active coupling.

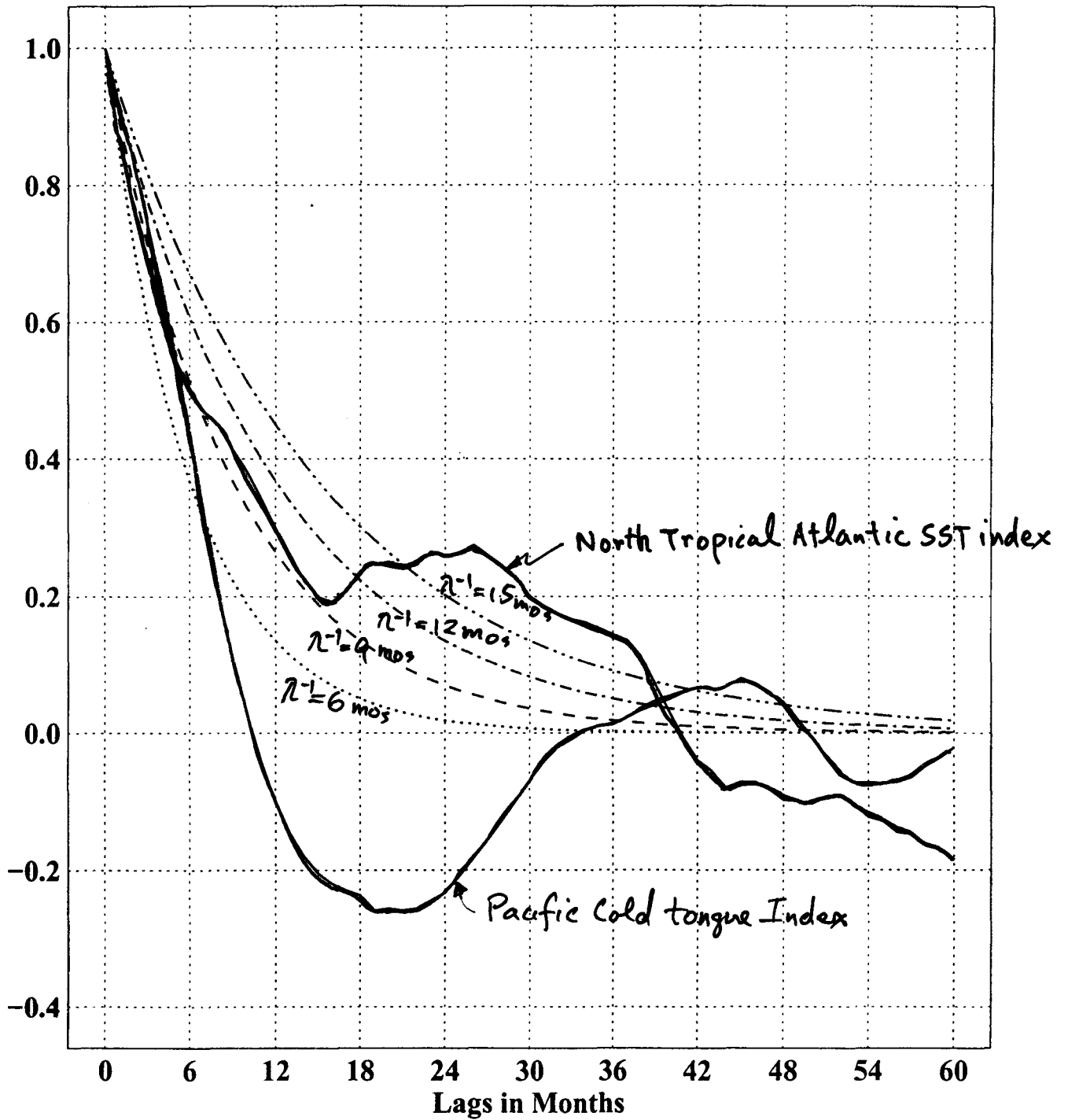
## Dynamic Feedbacks :

1. Bjerknes feedback: Trade Winds  $\Rightarrow$  Thermocline  $\Rightarrow$  SST  $\Rightarrow$  Convection  $\Rightarrow$  Trade Winds
2. Ekman feedback: Cross-Equatorial Winds  $\Rightarrow$  Ekman Divergence/Convergence  $\Rightarrow$  SST  $\Rightarrow$  Boundary Layer Pressure  $\Rightarrow$  Cross-Equatorial Winds

## Thermodynamic Feedbacks :

1. Wind-Evaporation-SST feedback: Winds  $\Rightarrow$  Evaporation/Latent Heat Flux  $\Rightarrow$  SST  $\Rightarrow$  Boundary Layer Pressure  $\Rightarrow$  Winds
2. Cloud-SST feedback: Cloud  $\Rightarrow$  Radiation  $\Rightarrow$  SST  $\Rightarrow$  Cloud

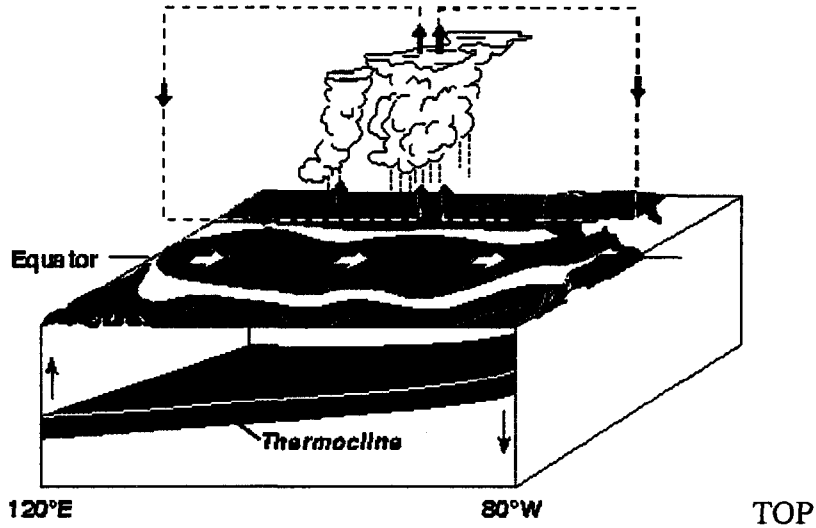
# SSTA Persistence (lag - auto correlation)



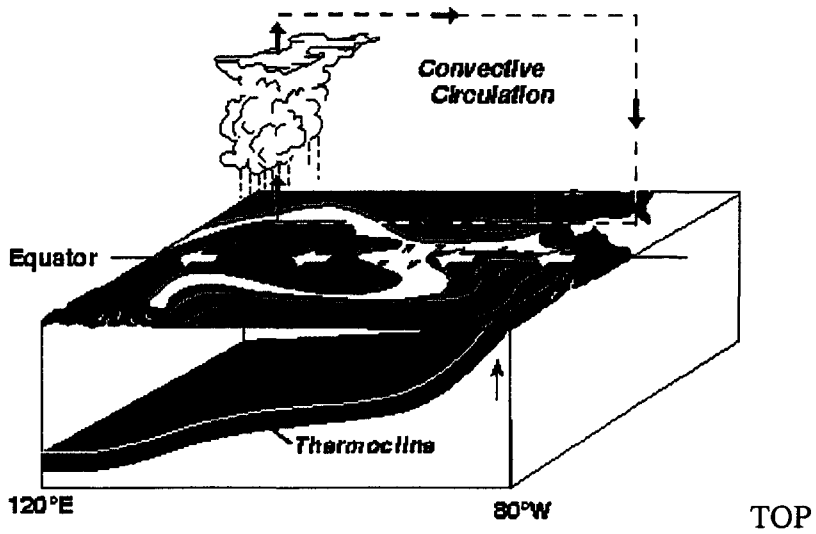
# El Niño Theme Page

Home | El Niño | Normal | La Niña

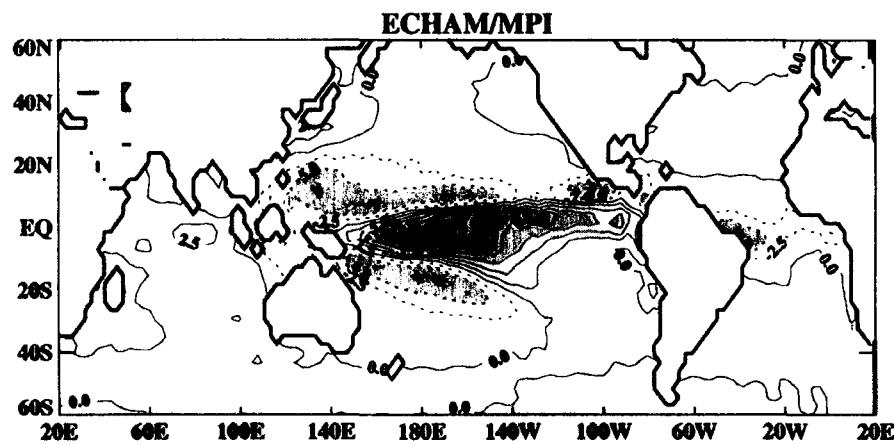
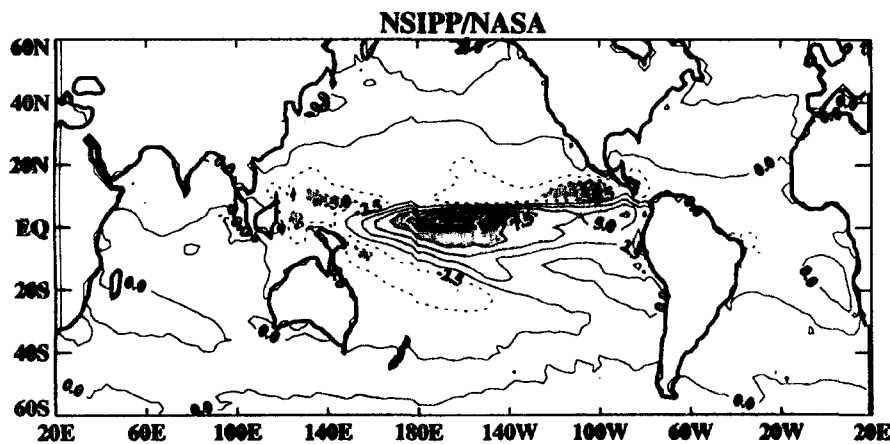
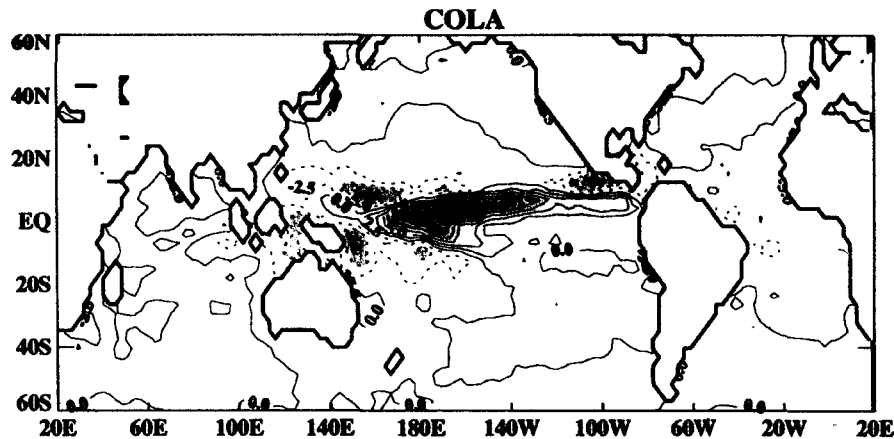
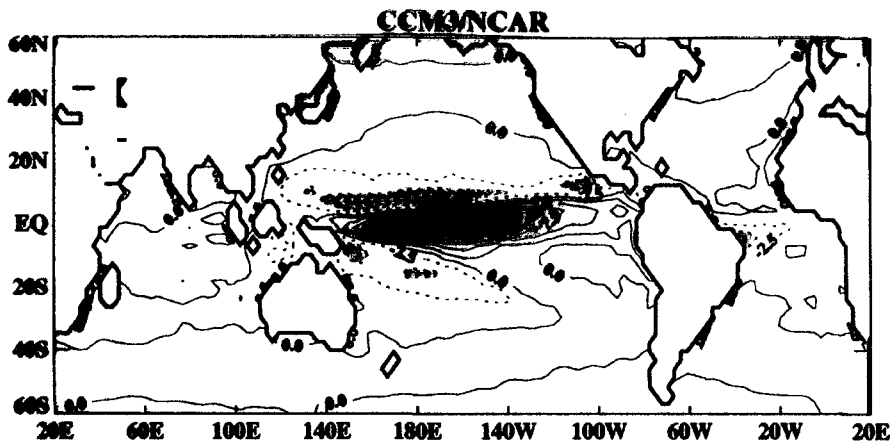
## El Niño Conditions



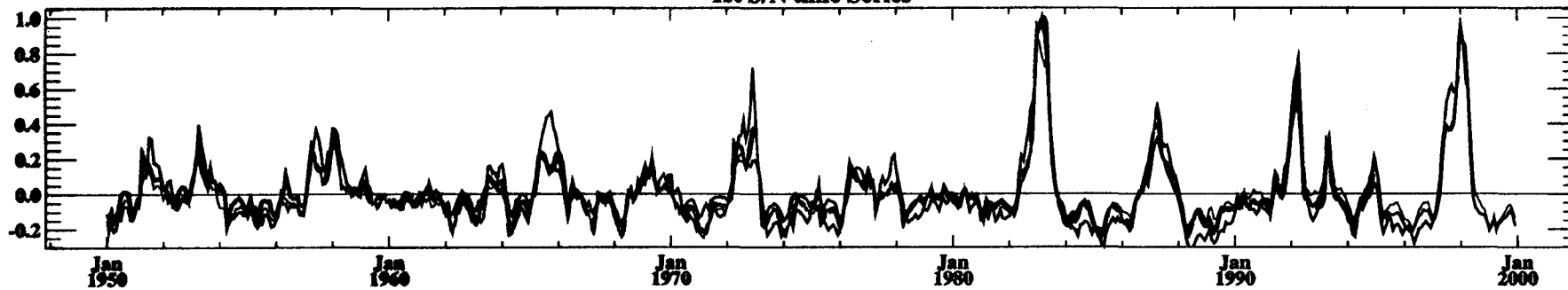
## Normal Conditions



### 1st S/N Pattern (Precipitation)



### 1st S/N time Series



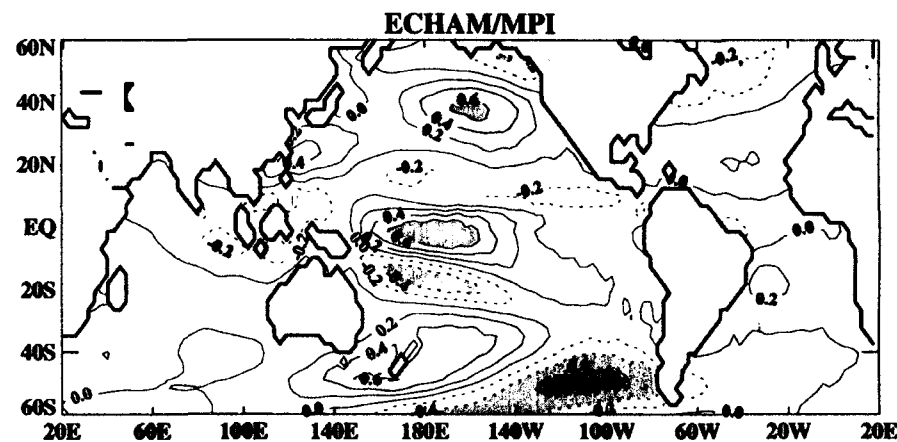
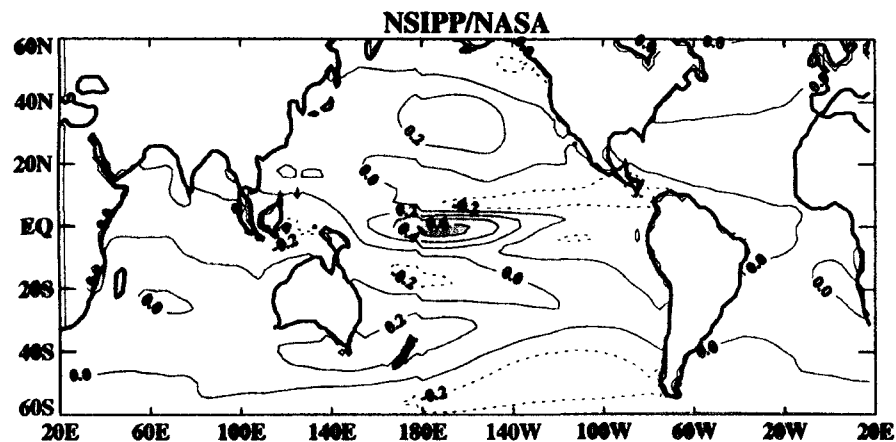
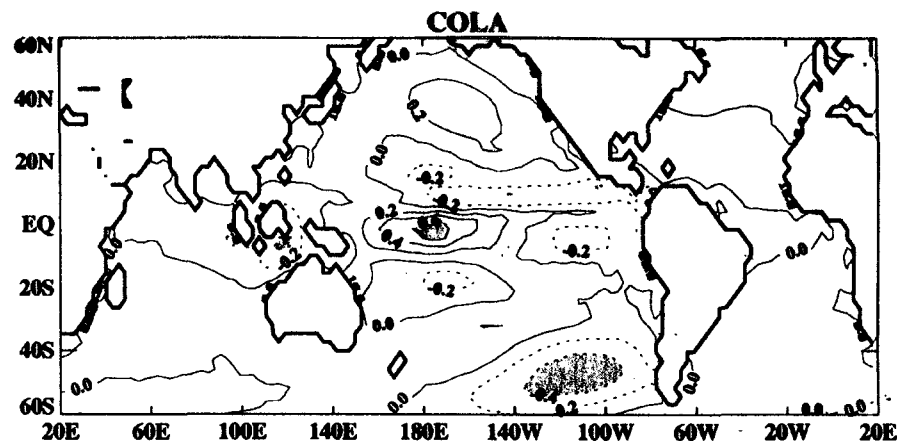
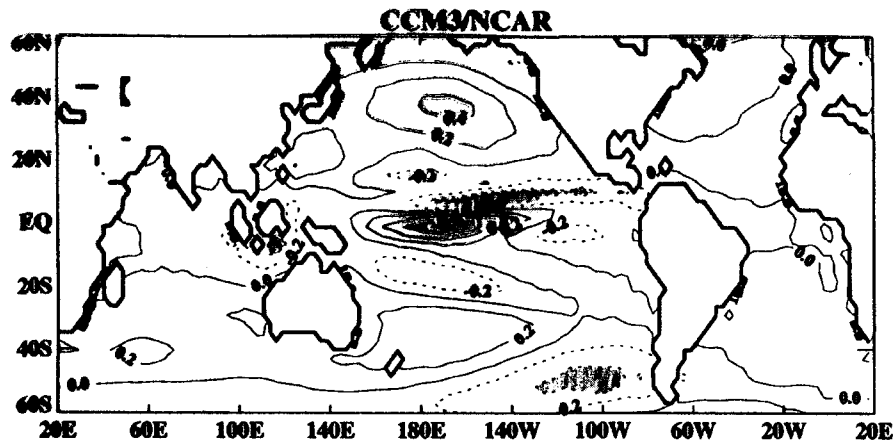
— CCM3

- - - COLA

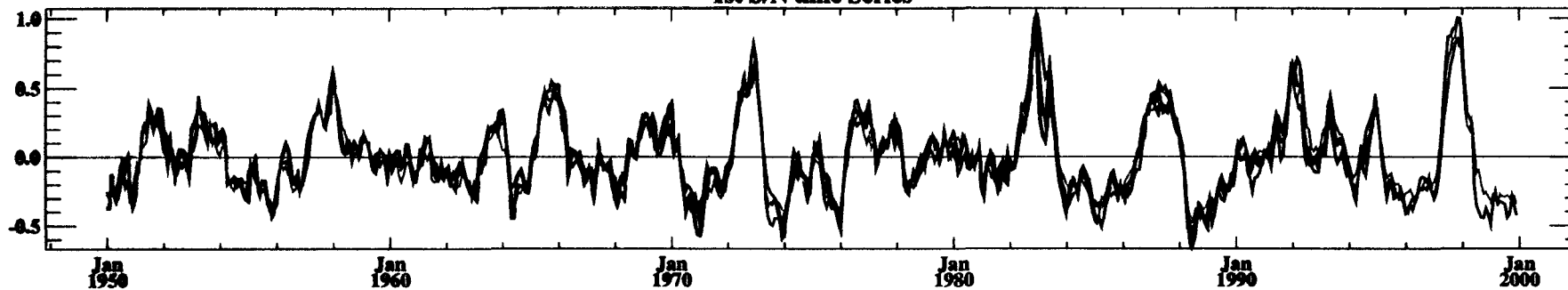
... NSIPP

- · - ECHAM

1st S/N Pattern (Taux)



1st S/N time Series



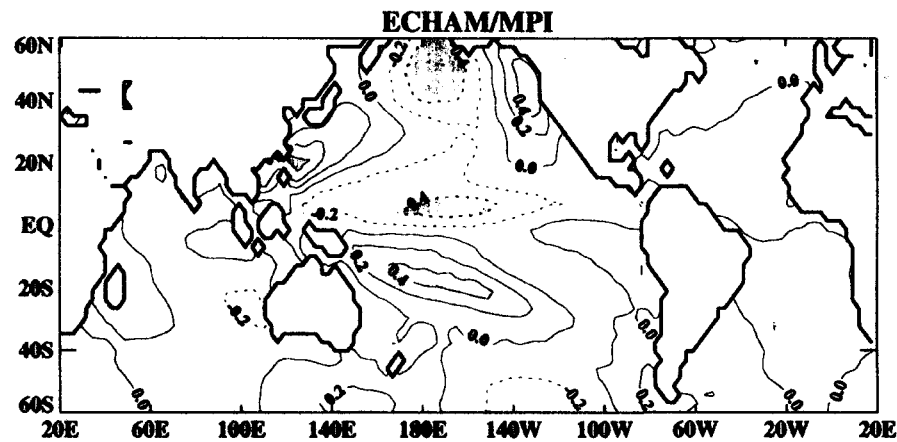
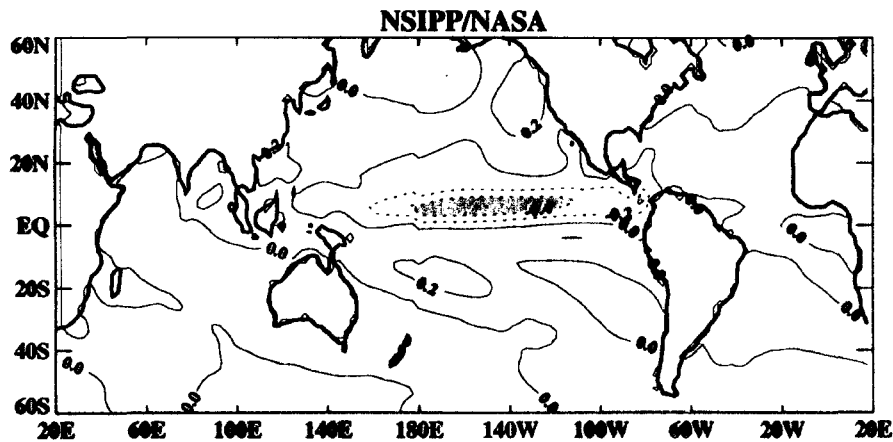
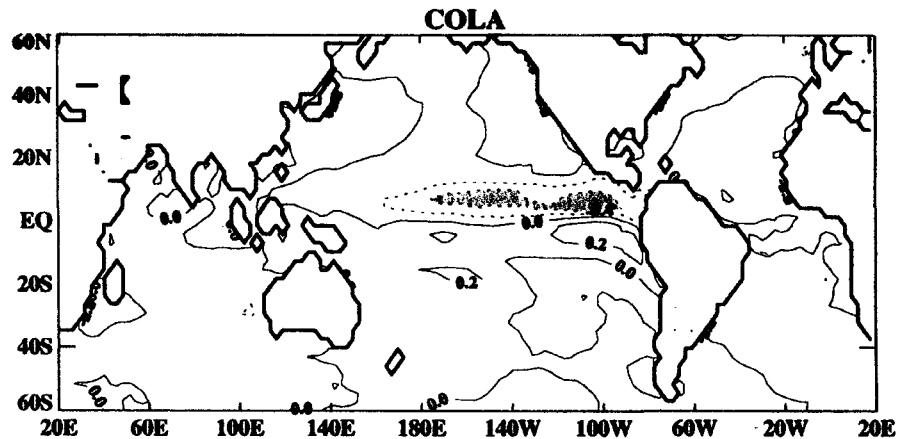
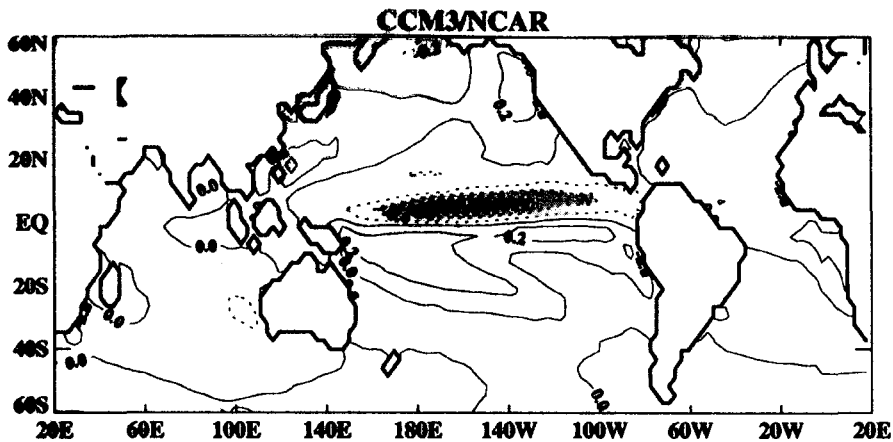
— CCM3

— COLA

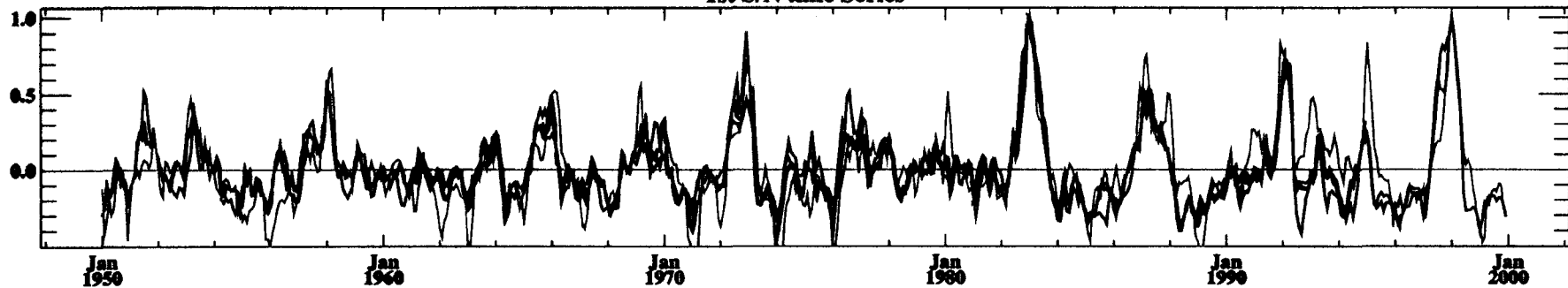
— NSIPP

— ECHAM

1st S/N Pattern (Tauy)

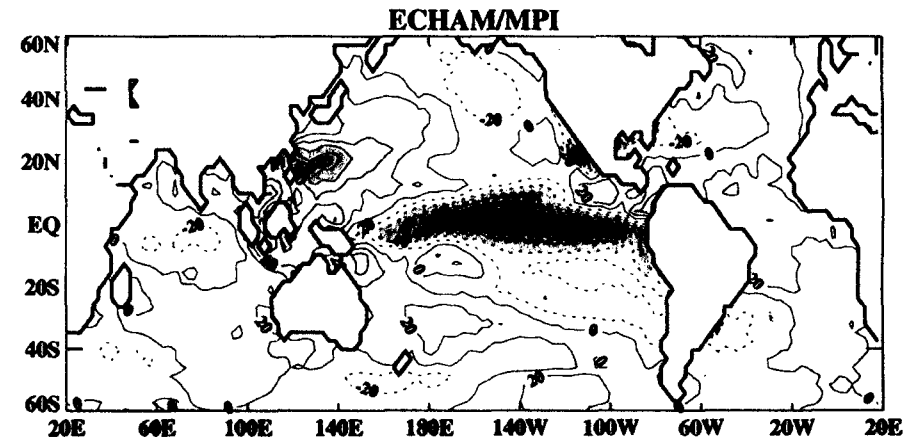
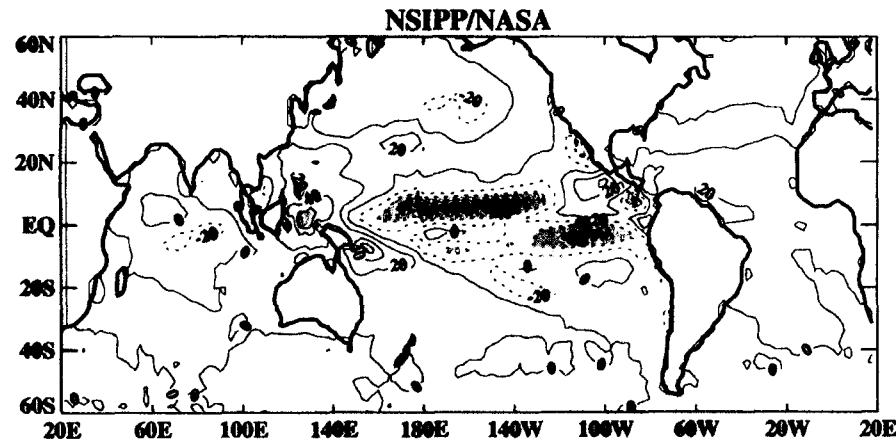
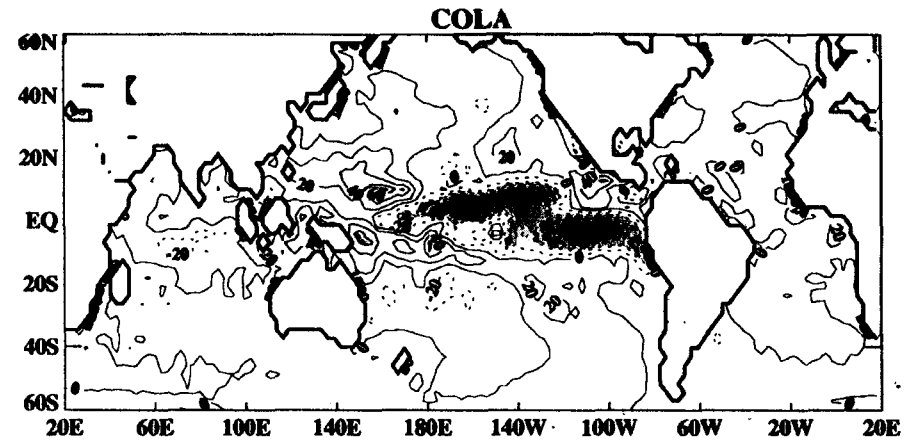
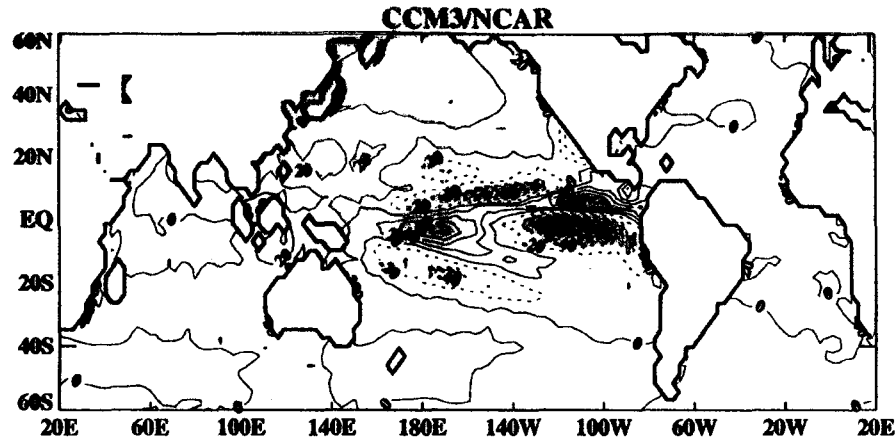


1st S/N time Series

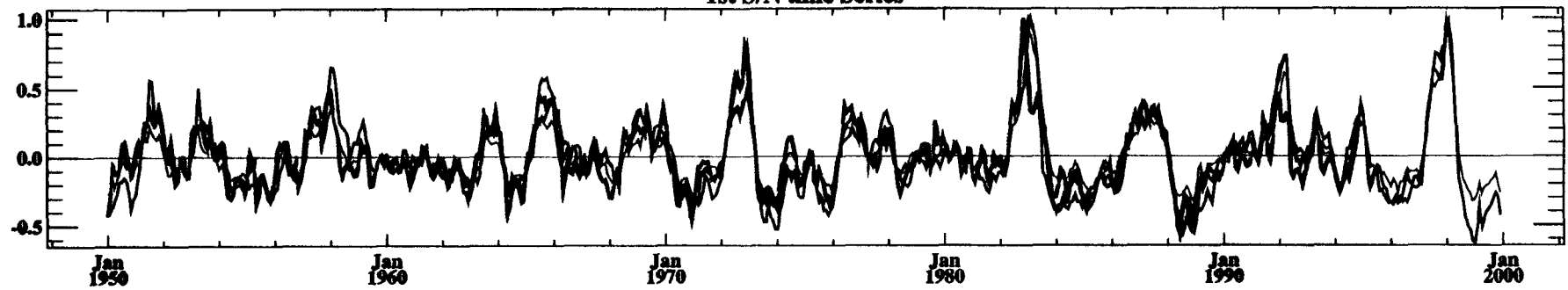


— CCM3      — COLA      — NSIPP      — ECHAM

### 1st S/N Pattern (Flux)

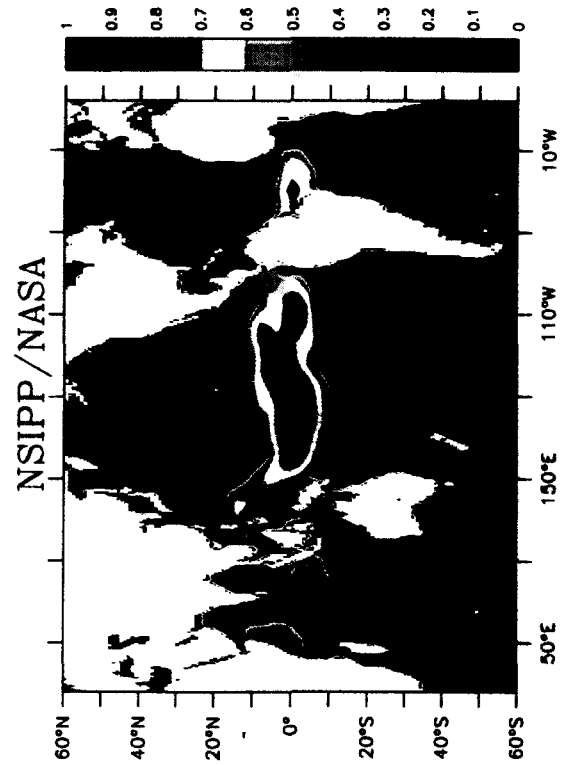
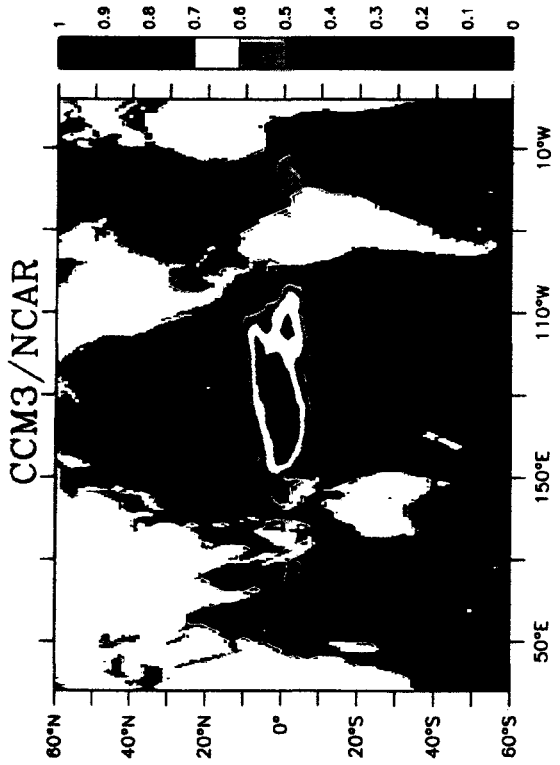
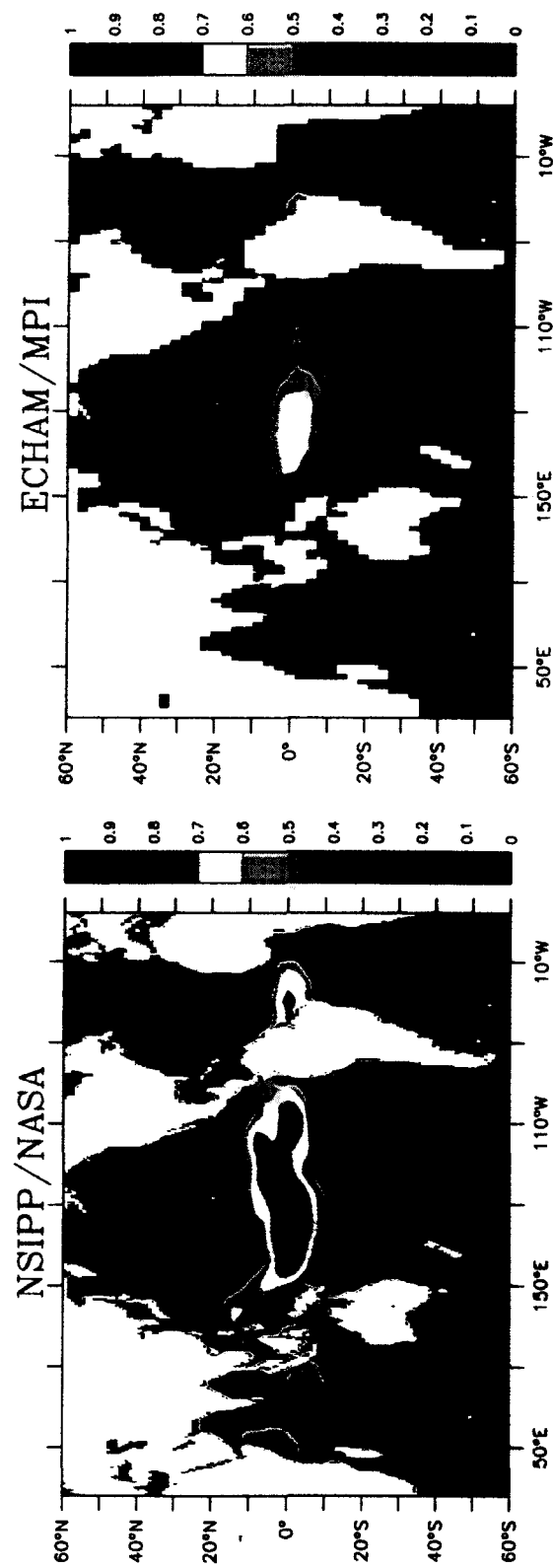
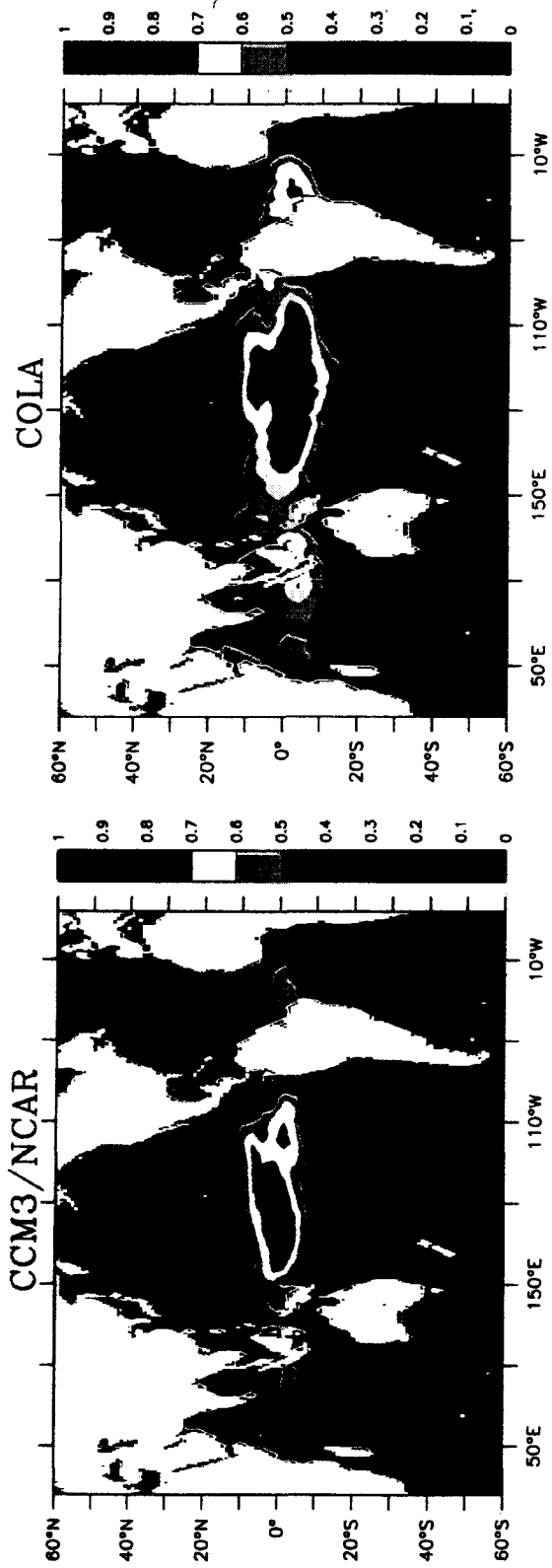


### 1st S/N time Series

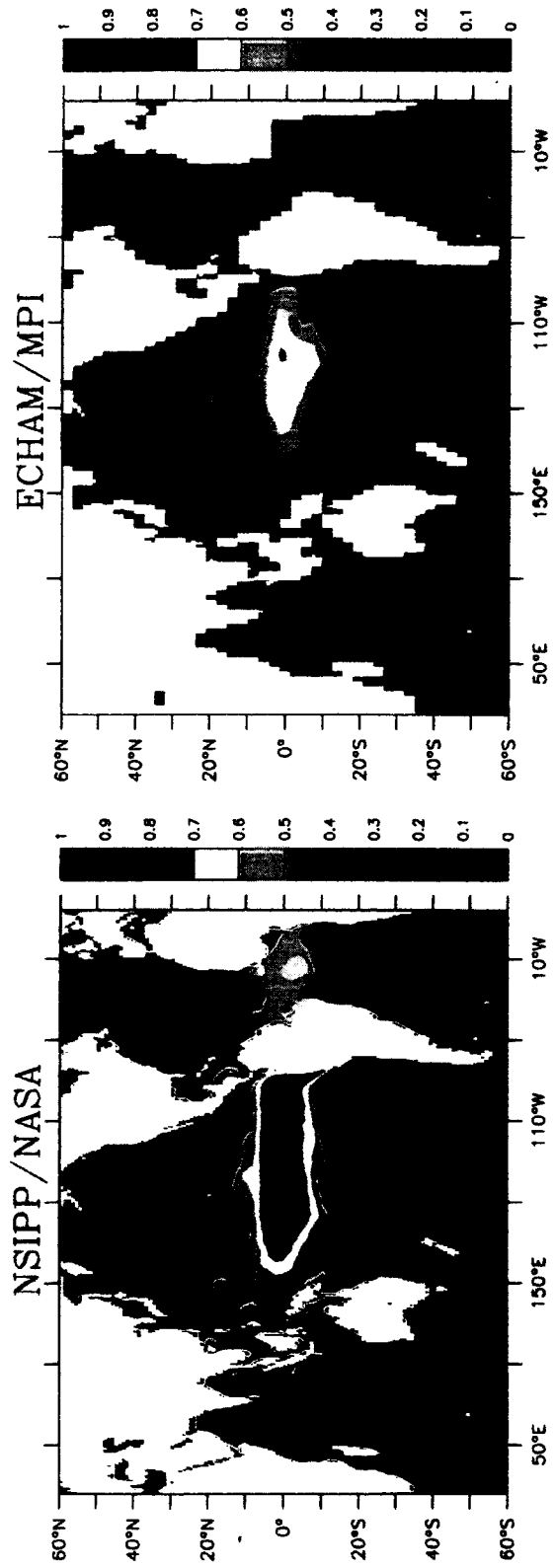
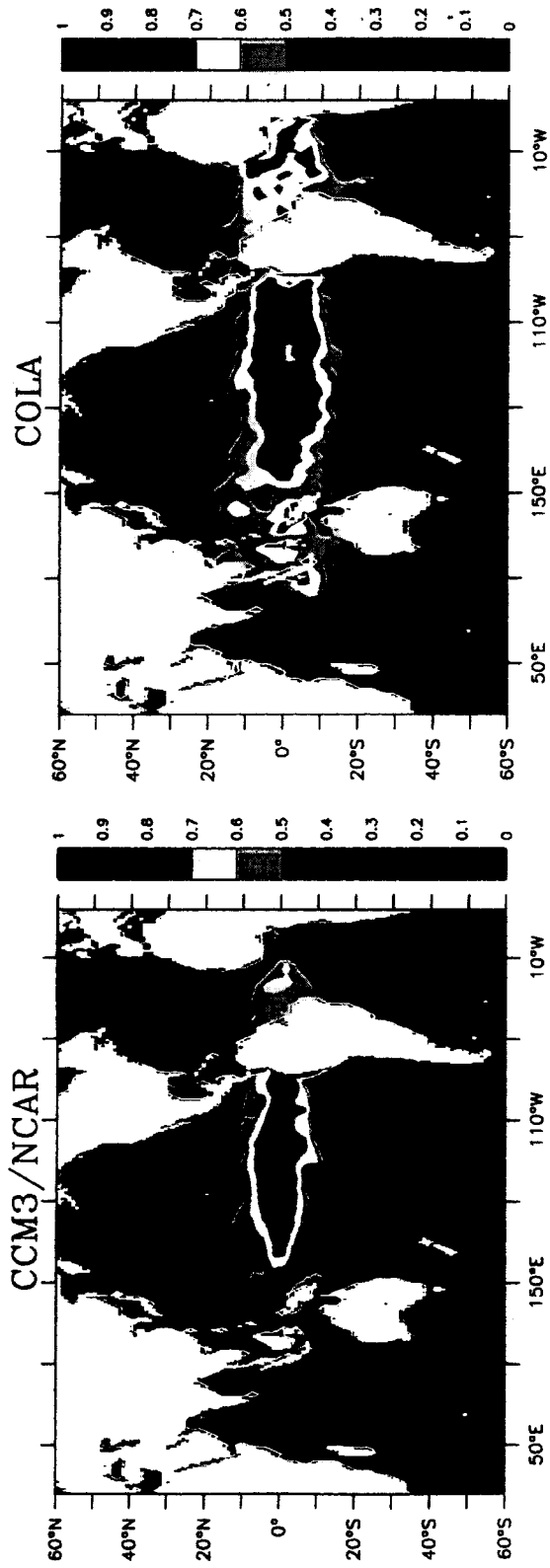


— CCM3 — COLA — NSIPP — ECHAM

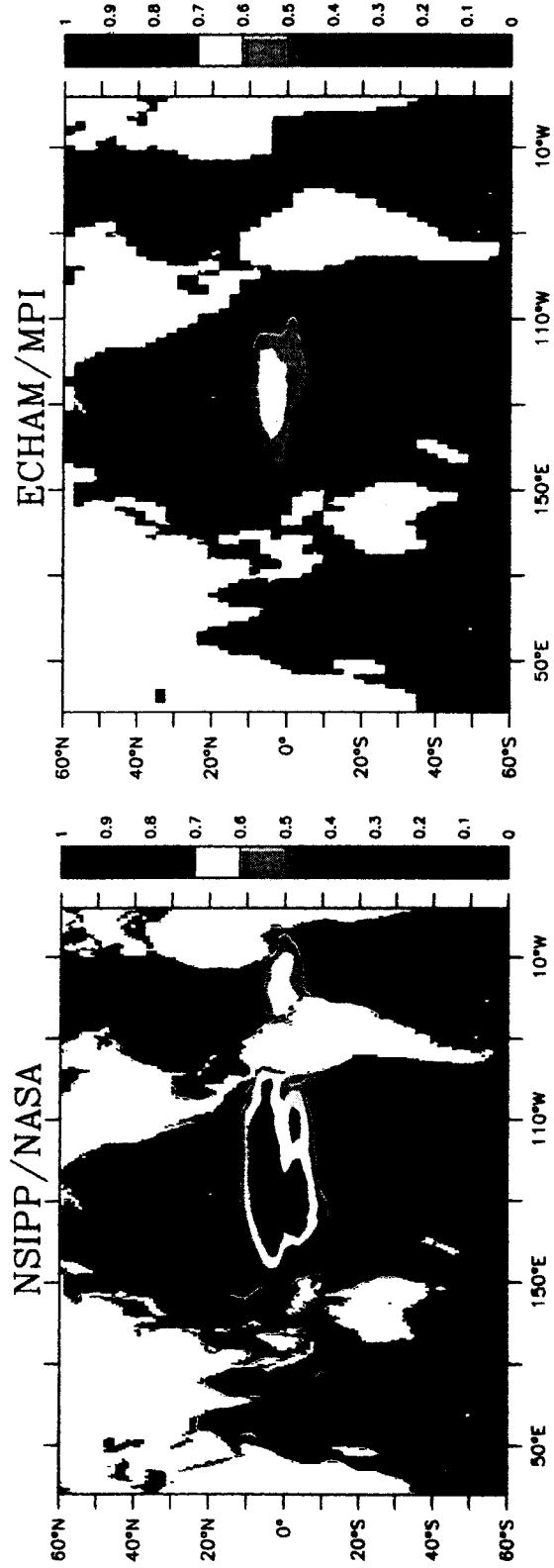
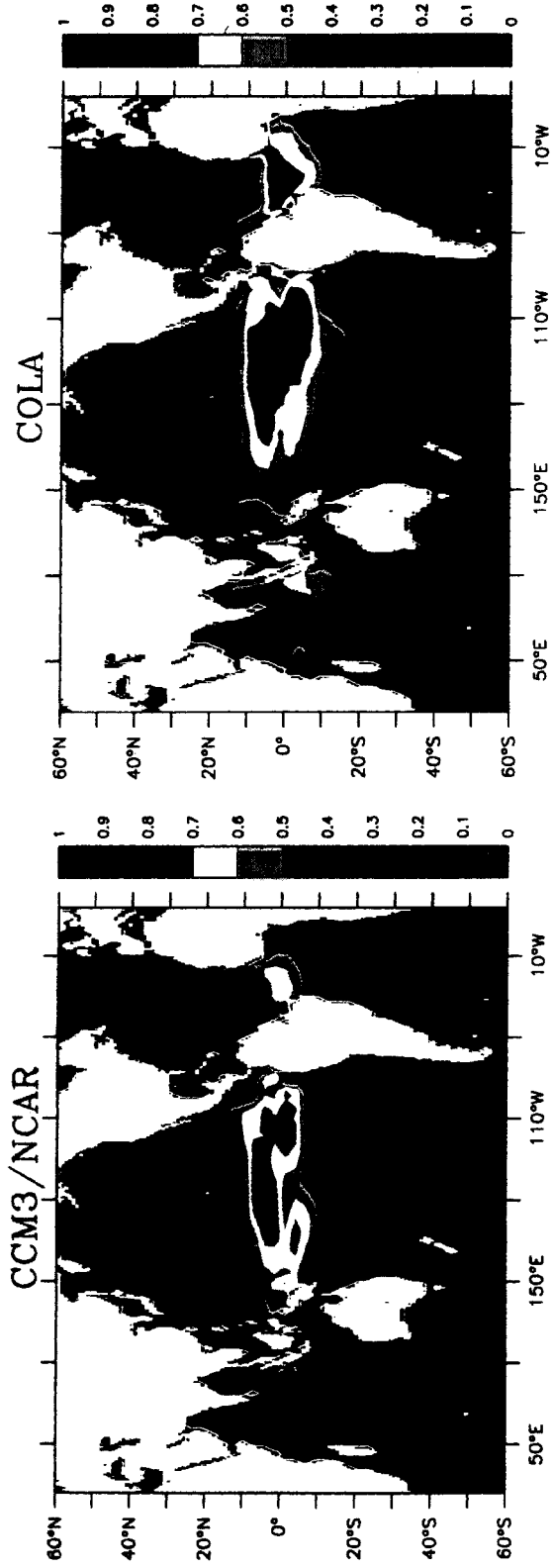
# Ratio of Signal/Total Variance (Taux)



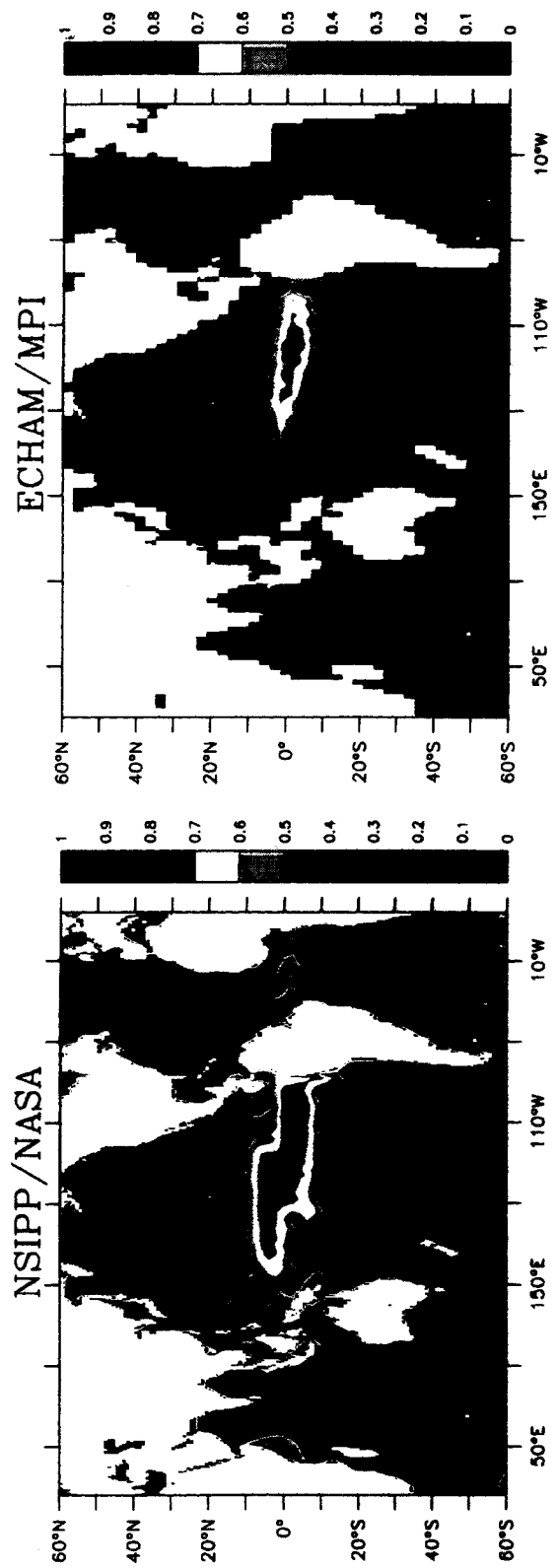
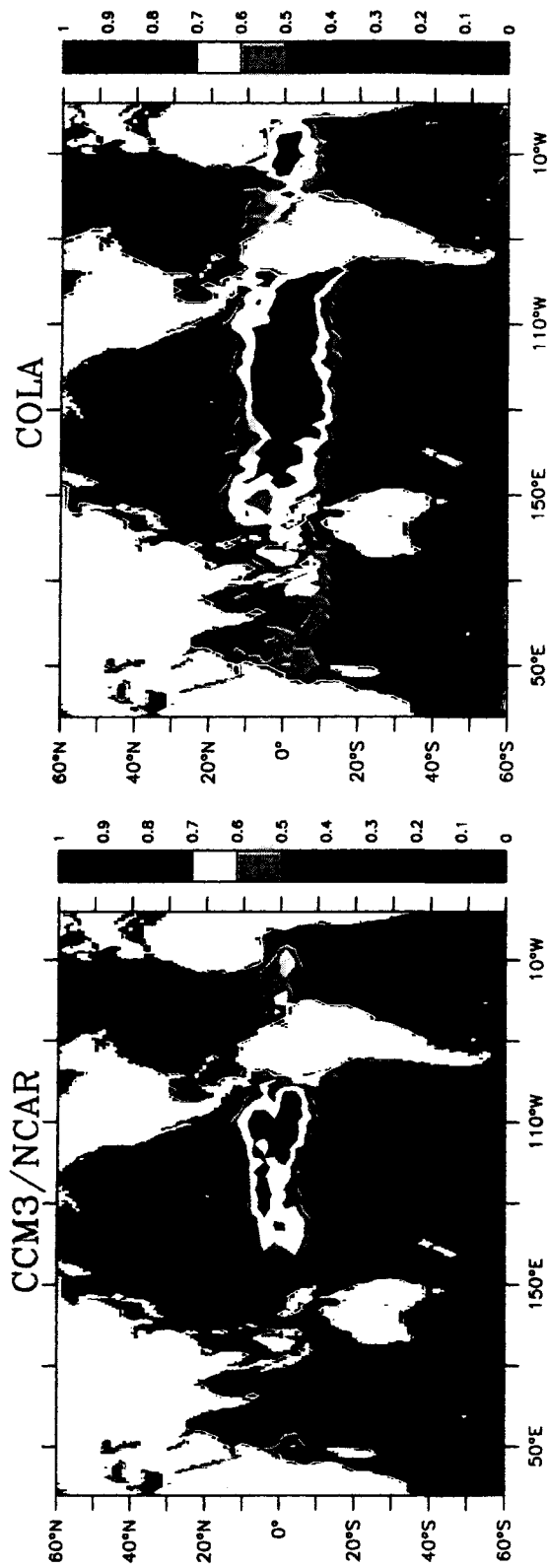
# Ratio of Signal/Total Variance (Precipitation)



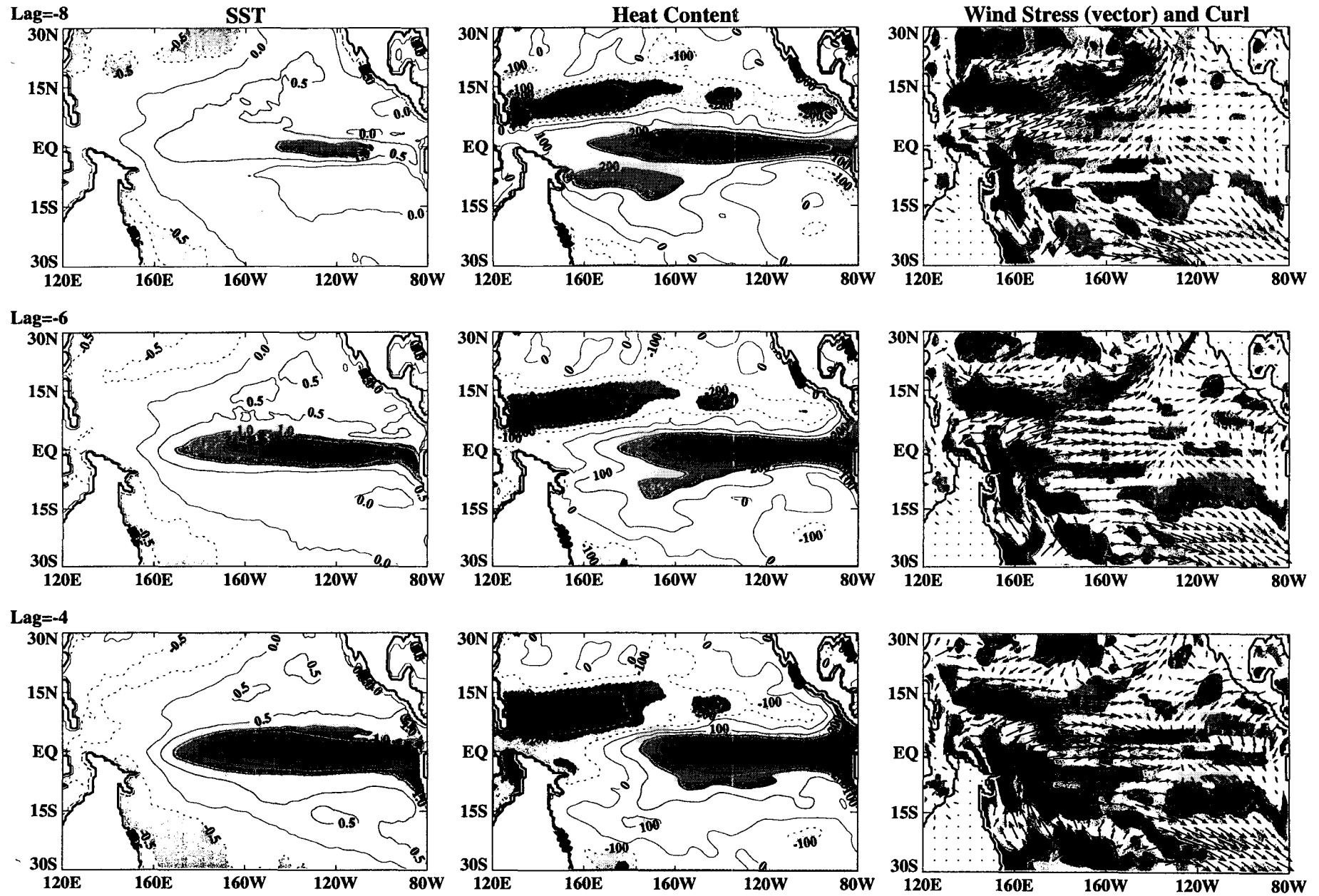
# Ratio of Signal/Total Variance (Tauy)



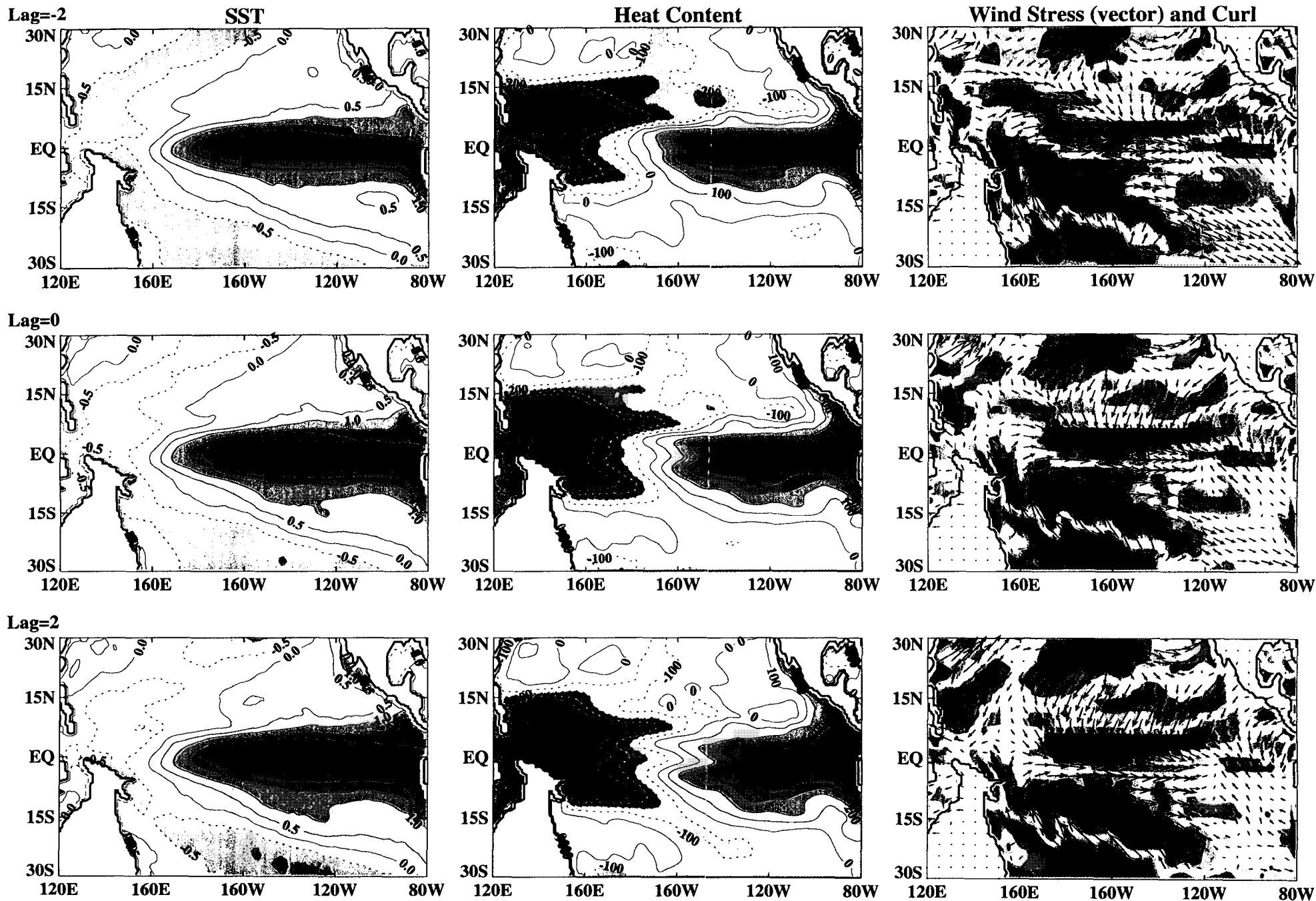
# Ratio of Signal/Total Variance (Flux)



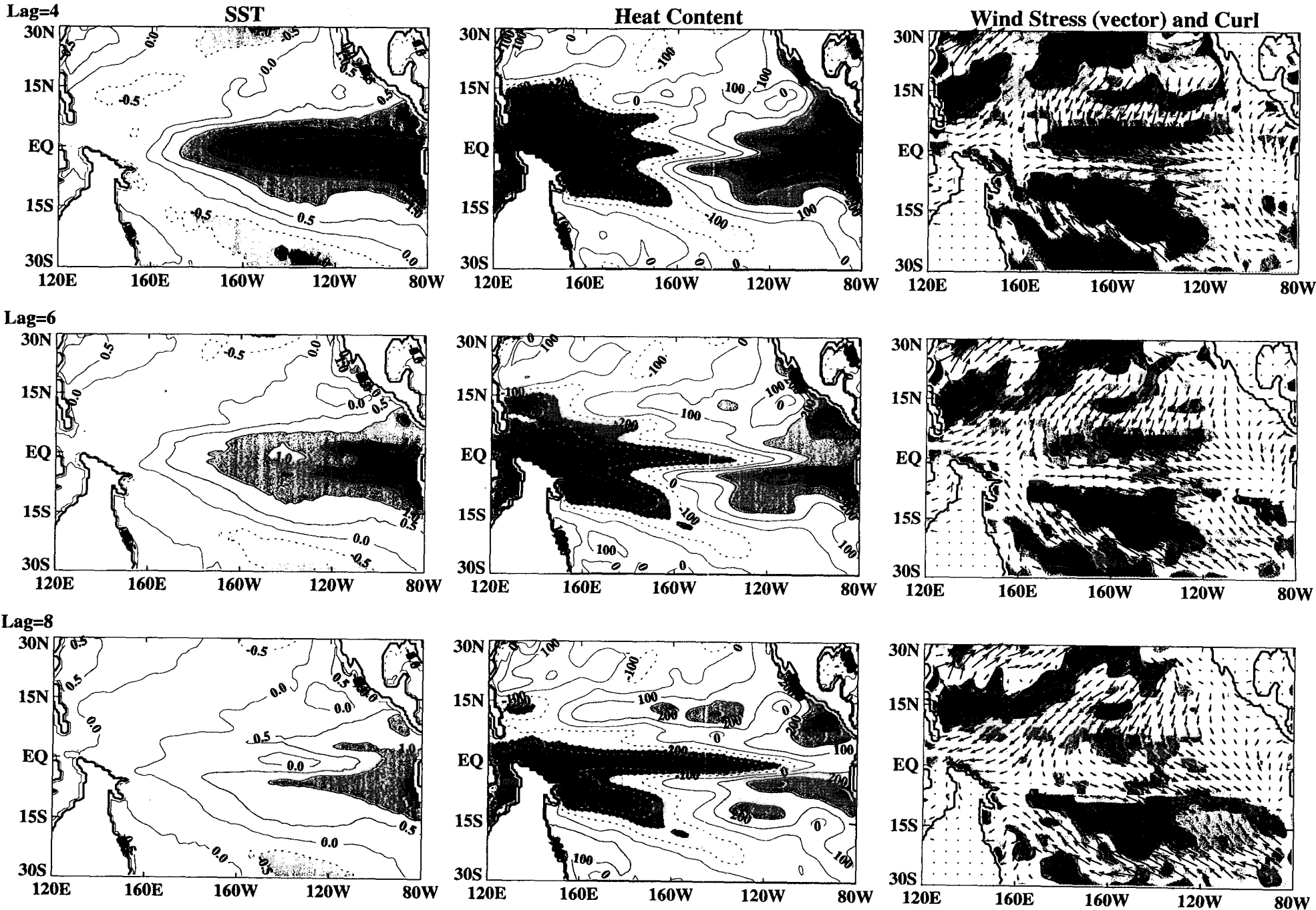
### Lag-Regression Analysis (GFDL Assimilation 1980-2000)



# Lag-Regression Analysis (GFDL Assimilation 1980-2000)



Lag-Regression Analysis (GFDL Assimilation 1980-2000)



Pacific

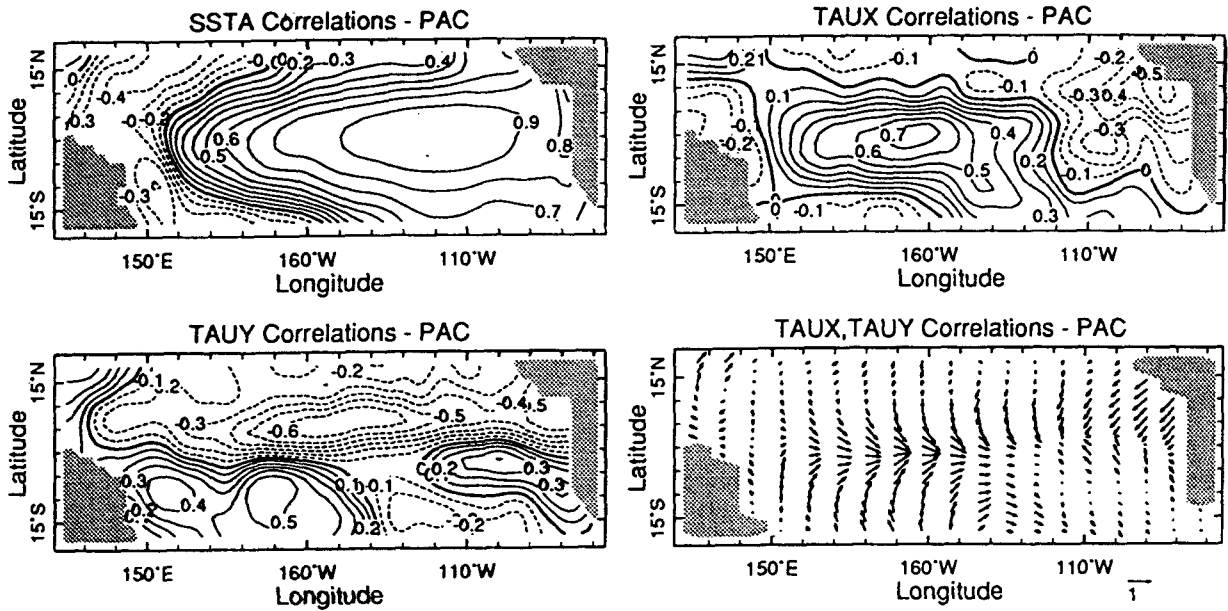


FIG. 1. Correlations between Pacific SST and pseudostress anomalies and the index NINO3. Lower-right panel presents the zonal and meridional component correlations as vectors.

Atlantic

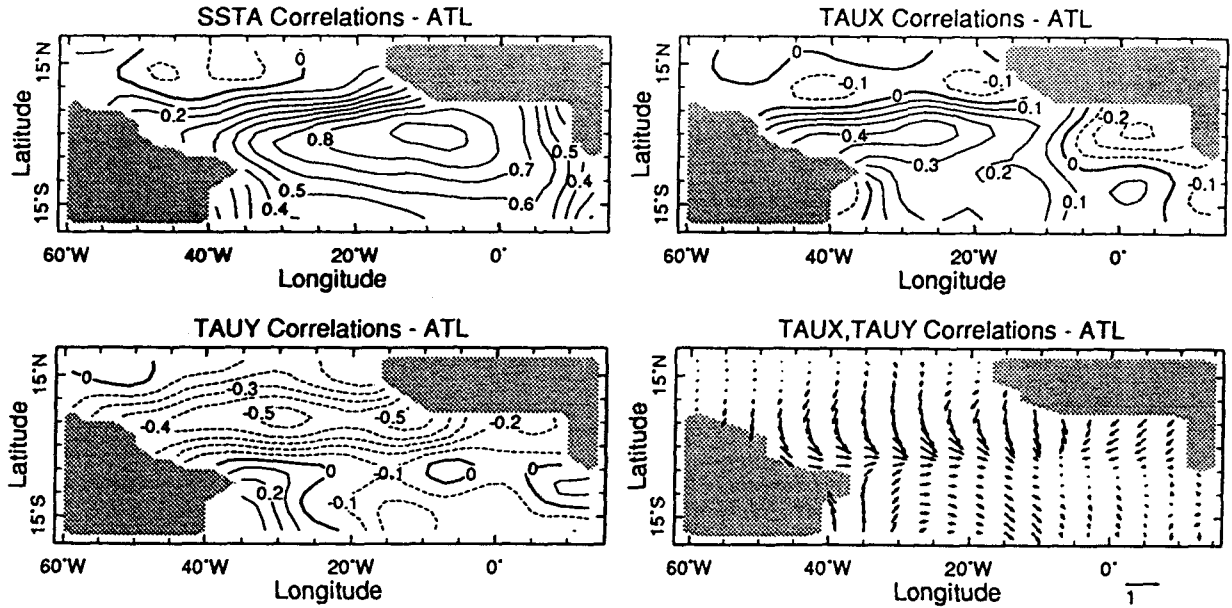
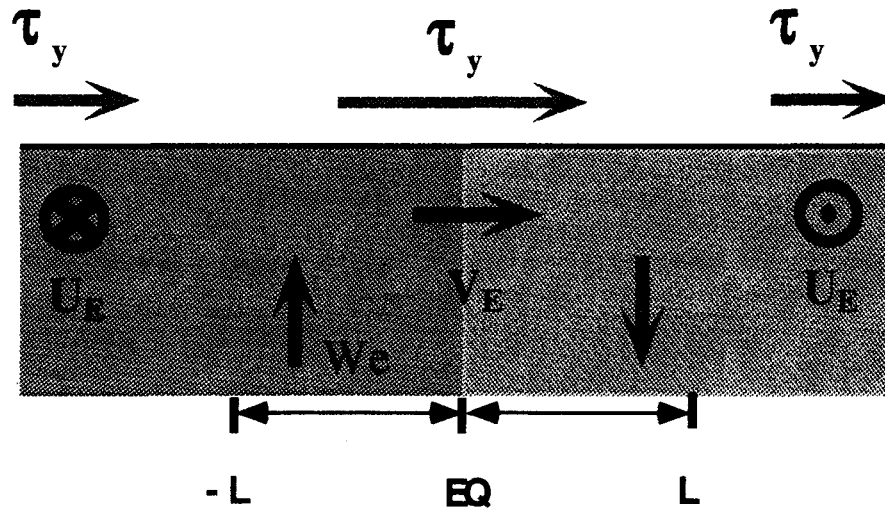


FIG. 2. Correlations between Atlantic SST and pseudostress anomalies, and the index ATL3. Lower-right panel presents the zonal and meridional component correlations as vectors.

# EKman Feedback

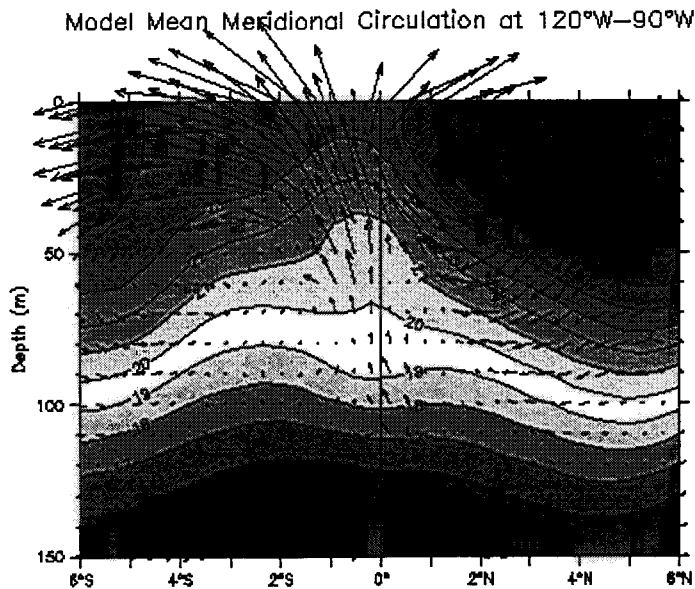


$$r_s V_E + f U_E = \tau_y$$

$$\text{If } |y| < L, \quad r_s V_E = \tau_y$$

$$\text{If } |y| > L, \quad f U_E = \tau_y$$

Kessler



to the presence of strong southerly cross-equatorial winds, and also to the deceleration of the equatorial undercurrent. In the central Pacific zonal winds are strong and meridional winds weak. This gives the classical symmetric Ekman divergence at the surface, with upwelling fed symmetrically by inflows at thermocline level from both hemispheres; the undercurrent not changing zonally so it removes about as much water as it brings in the region.

In the east, on the other hand (this figure), southerly winds create a northward cross-equatorial current that distorts the meridional symmetry; in addition upwelling is fed not so much by meridional inflows as by water leaving the slowing undercurrent.

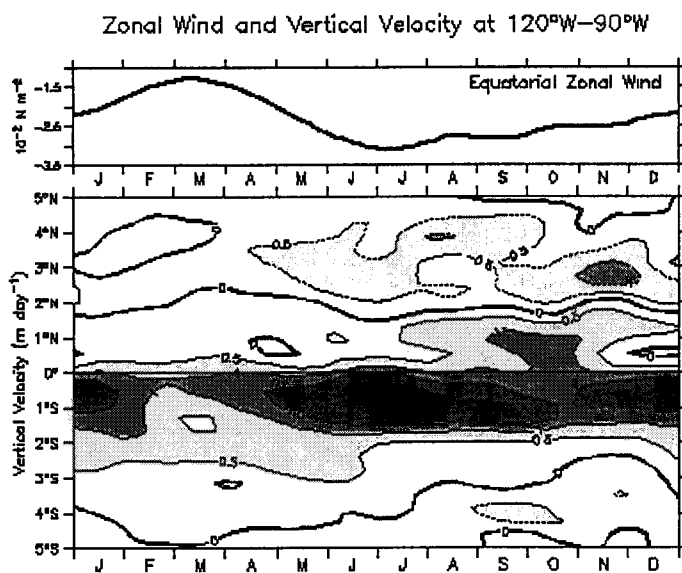


Figure 5. Upwelling roughly doubles (to more than 2 meters/day) when winds are strong, as so is a large cooling term in the second half of the year. Thus upwelling cools the ocean at the same time that solar radiation is blocked by clouds. Strong winds also produce an increase in evaporation at this time, which amplifies the cooling.

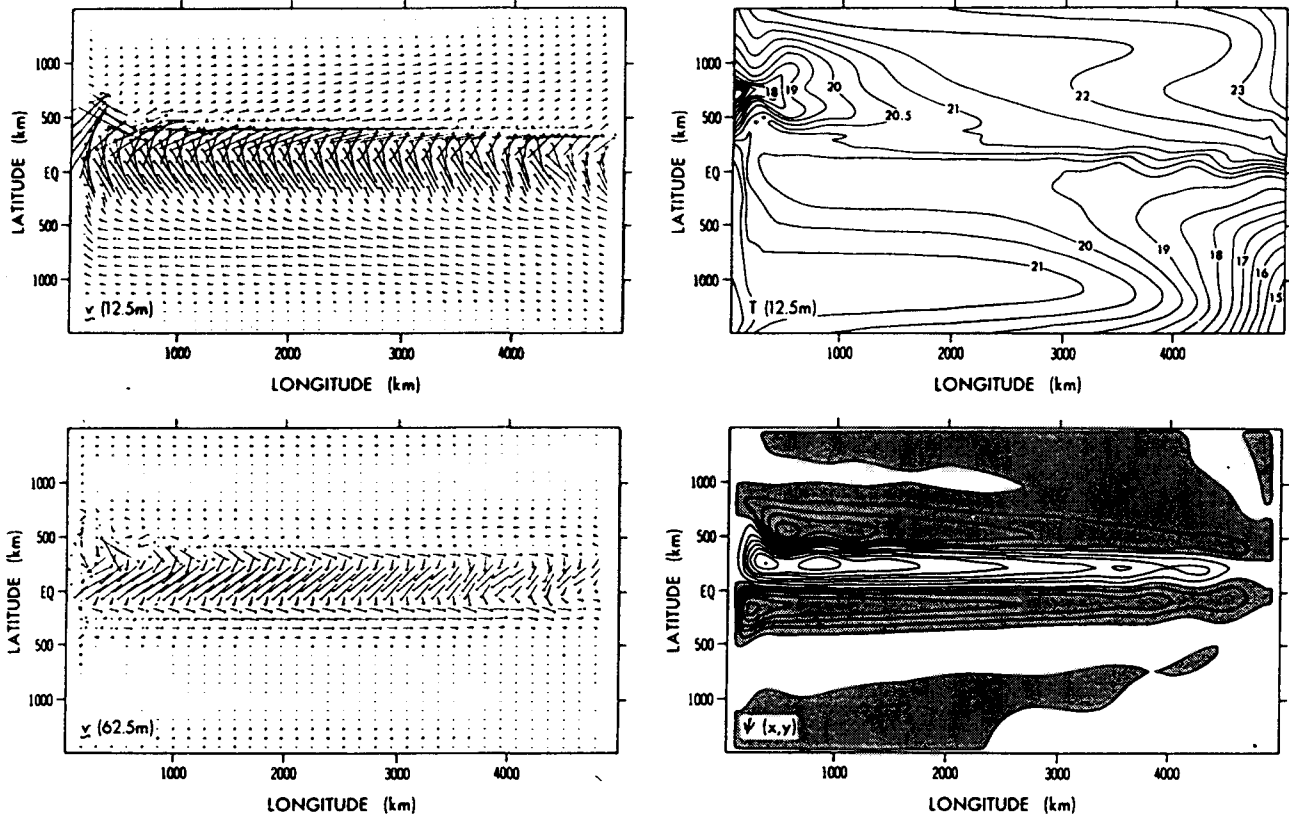
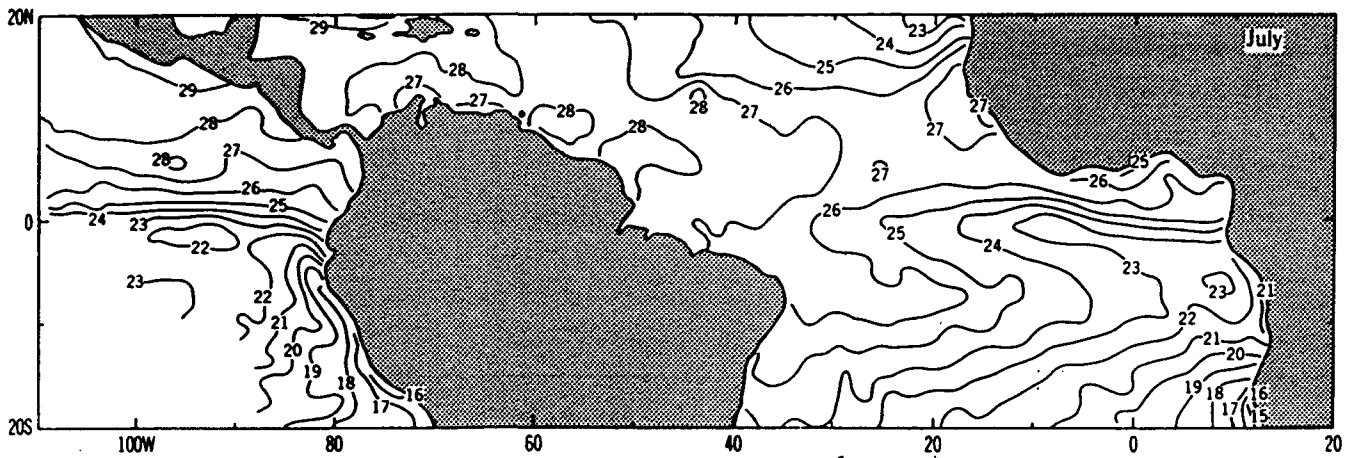


Fig. 4. The left-hand panels show horizontal velocity vectors at depths of 12.5 m (top) and 62.5 m (bottom). The right-hand panels show the temperature at a depth of 12.5 m and the vertically integrated transport stream function  $\psi$ . (Contours are in units of  $10^6 \text{ m}^3/\text{s}$ .) These are instantaneous values at day 200.



## Bulk Formulae of Heat Fluxes

**Components of Heat Flux :** The net heat flux at the sea-surface consists of four components: shortwave radiation  $Q_{sw}$ , long-wave radiation  $Q_{lw}$ , latent heat flux  $Q_{lh}$  and sensible heat flux  $Q_{sh}$ , i.e.,

$$Q_{net} = Q_{sw} - Q_{lw} - Q_{lh} - Q_{sh}. \quad (6)$$

**Radiative Fluxes  $Q_{sw}$  &  $Q_{lh}$  :**  $Q_{sw}$  depends on cloud cover  $C$ , and increases as  $C$  decreases:

$$Q_{sw} = 0.94I_0(1 - 0.62C + 0.00019\theta), \quad (7)$$

where  $I_0$  is the solar radiation,  $\theta$  is the noon solar altitude, and  $C$  is the total cloud cover.

$Q_{lw}$  anomalies are usually quite small on monthly time-scale.

**Latent Heat  $Q_{lh}$  and sensible heat  $Q_{sh}$  :**

$$Q_{lh} = \rho L C_E (w \Delta q), \quad (8)$$

$$Q_{sh} = \rho C_p C_H (w \Delta T), \quad (9)$$

where  $w$  is the total wind speed,  $\Delta q$  is the surface saturated humidity and air humidity difference, and  $\Delta T$  is the air-sea temperature difference.

$$Q'_{lh} \propto \langle w \rangle \Delta q' + w' \langle \Delta q \rangle, \quad (10)$$

$$Q'_{sh} \propto \langle w \rangle \Delta T' + w' \langle \Delta T \rangle, \quad (11)$$

$\Delta q'$  and  $\Delta T'$  are usually correlated, so

$$Q'_{lh} + Q'_{sh} \propto \langle w \rangle \Delta T' + w' \langle \Delta T \rangle. \quad (12)$$

Here  $\langle \rangle$  denotes time mean.

Note that the first term on RHS is the passive feedback in the energy balance model.

Latent and Sensible Heat Flux Variability / 23

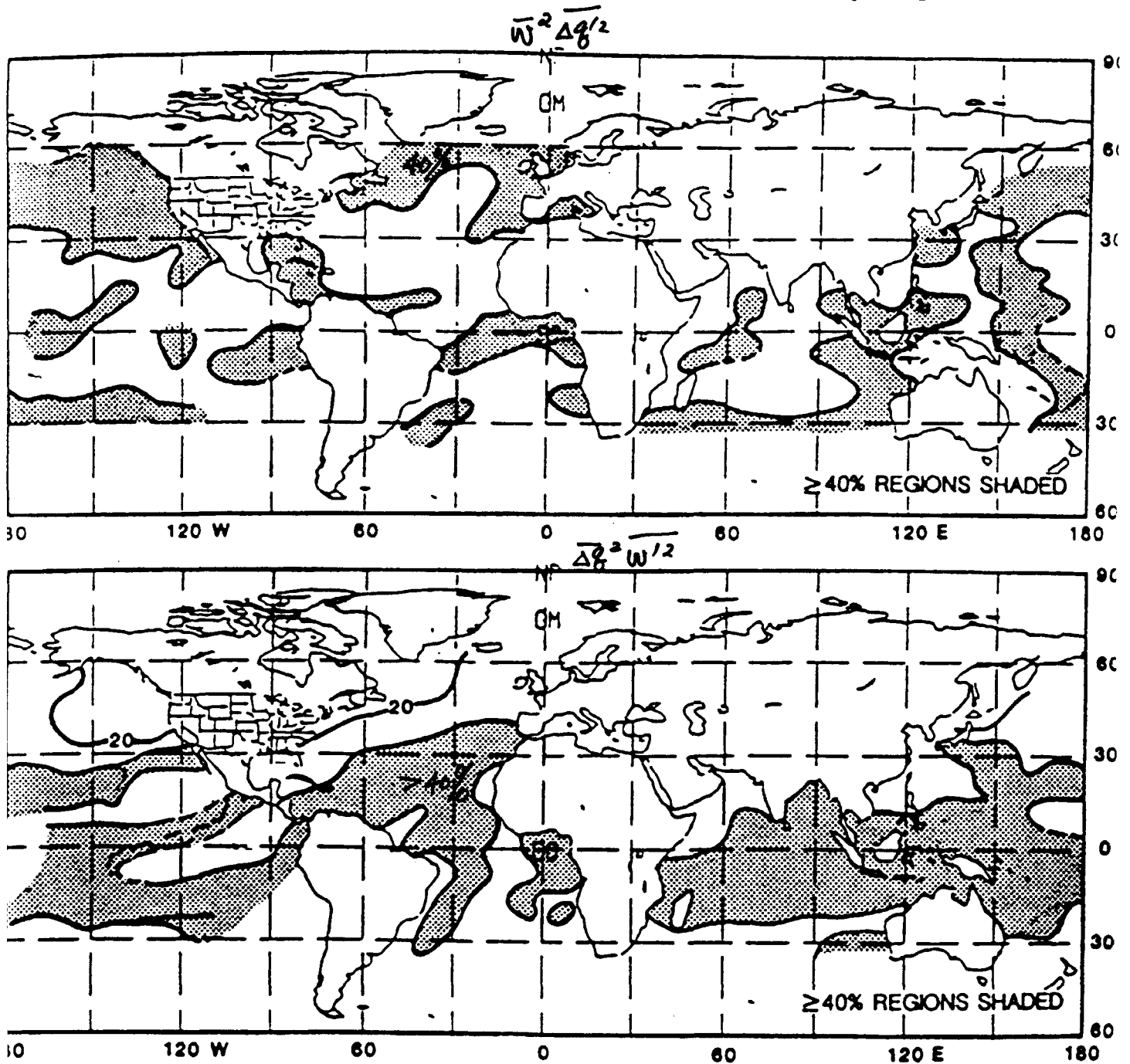


Fig. 7 Fraction (%) of  $F_1$  variance,  $\sigma_{F_1}^2$ , contributed by  $\bar{w}^2 \overline{\Delta q'^2}$  (above) and by  $\overline{\Delta q'^2} \bar{w}'^2$  (below) computed from December, January and February 1950–1986 data. Shading indicates region with 40% of variance explained.

$\Delta q' \sim \Delta T'$   
 $\Delta q' \sim w'$

Latent and Sensible Heat Flux Variability / 25

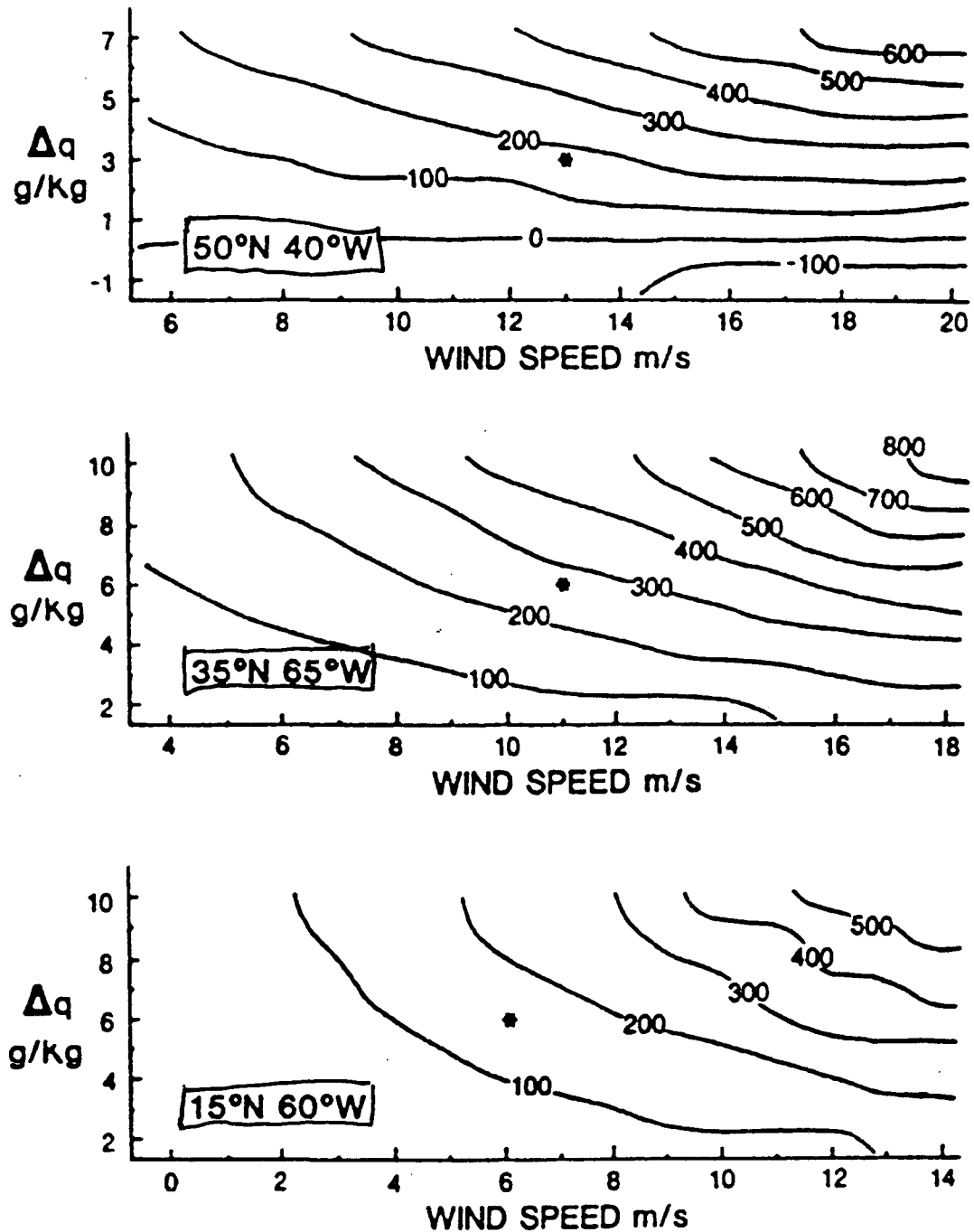
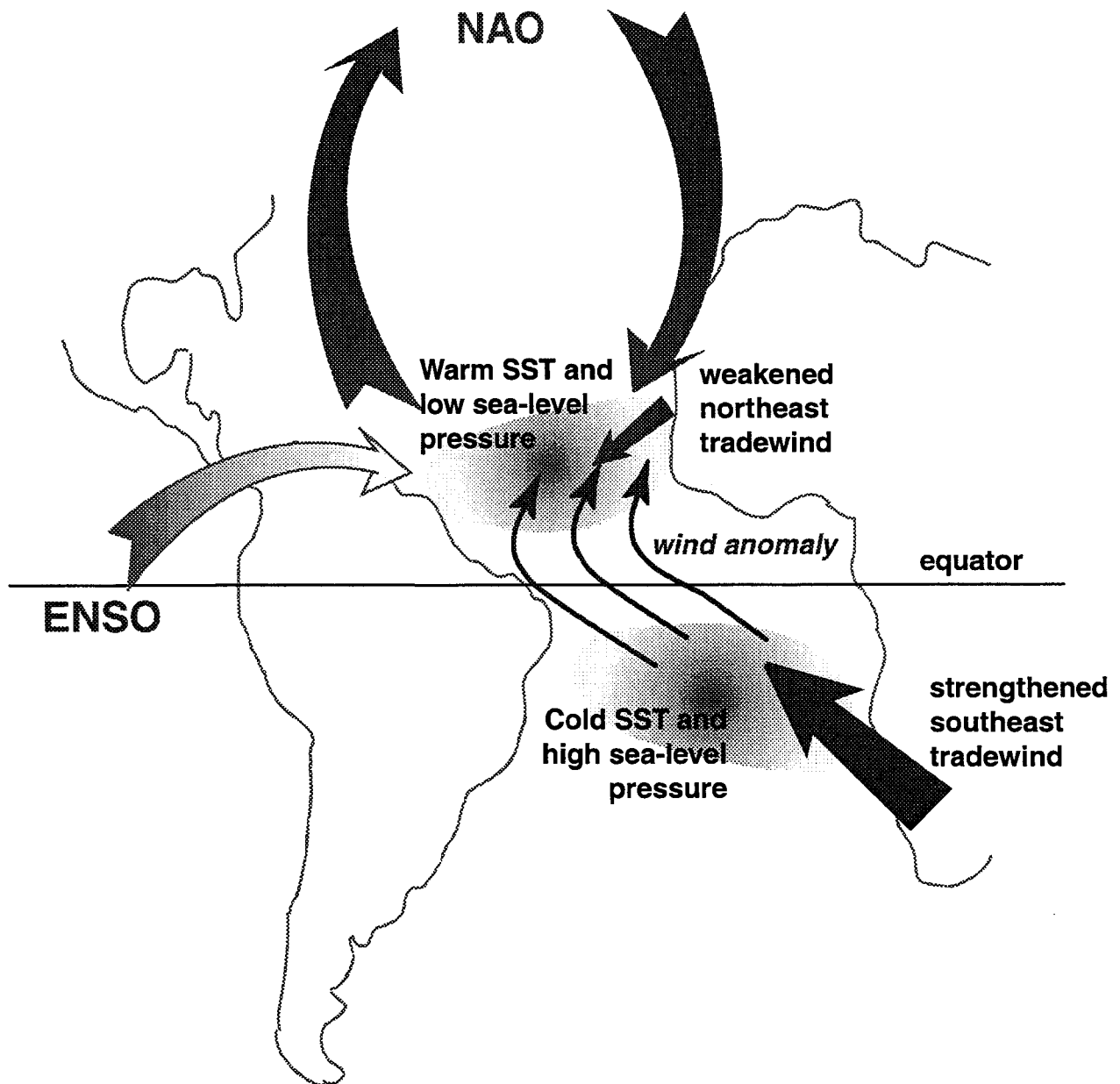
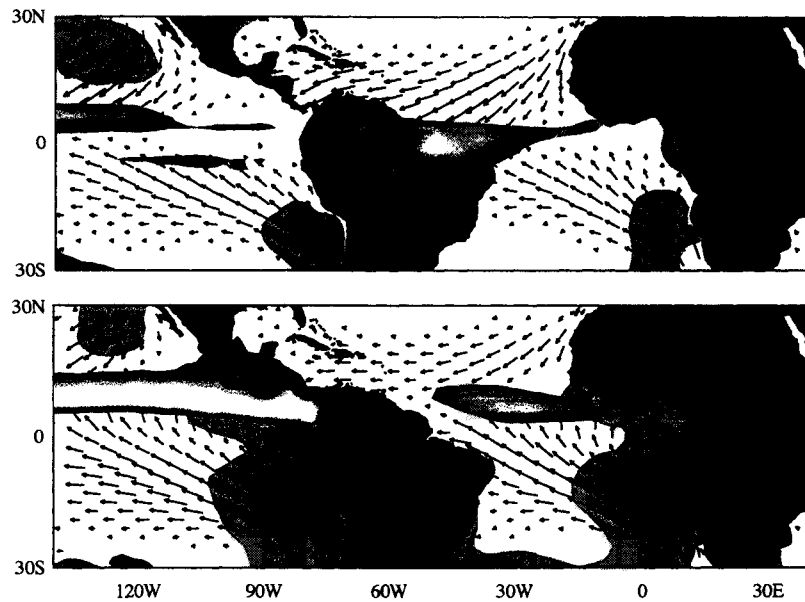


Fig. 9 Latent flux dependence ( $W m^{-2}$ ) on  $w$  and  $\Delta q$  for three selected North Atlantic grid points. Variations in  $w$  and  $\Delta q$  are anomalies about the January long-term mean condition, indicated by an asterisk.

# Mechanisms of Tropical Atlantic Variability





**Figure 9.** As in Fig. 2, but for the March-April mean (upper panel and September-October mean conditions (lower panel). Note the double ITCZ configuration in the Pacific, symmetric about the equator in March-April, in contrast to the prominent single ITCZ near 10°N in September. A strongly contrasting structure is also observed in the Atlantic sector, with the ITCZ displaced farther north in September-October. Rainfall rates in excess of 20 cm per month are colored orange-yellow.

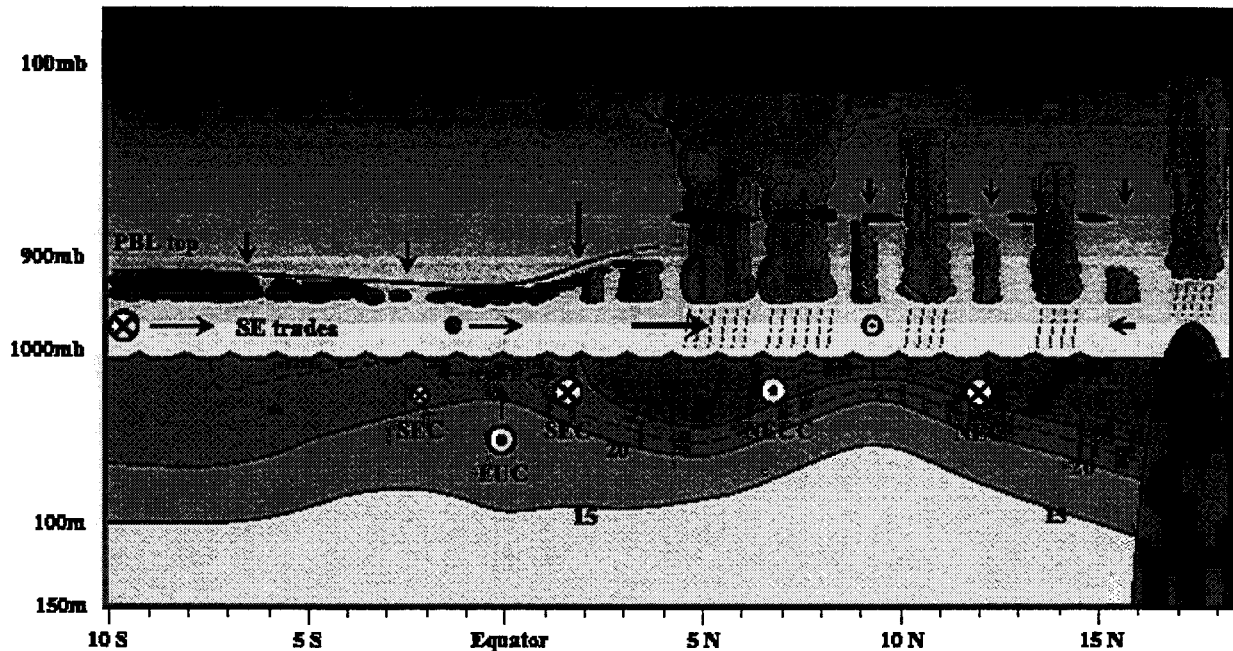


Figure 1. (Courtesy of S. Esbensen, Oregon State Univ). The important processes are illustrated in this schematic. At the equator, upwelling, extensive cloudiness and evaporation cool the SST, while mixing due to tropical instability waves across the strong front just north of the equator opposes these tendencies. These processes are difficult to determine observationally, due to our inability to measure upwelling, uncertainty about the complicated feedbacks between cloudiness and SST, and the sampling problem in estimating the heat fluxes due to the complicated three-dimensional structure of tropical instability waves. For these reasons resort to a numerical model is necessary.

The following figures are reduced in size. Click on the figure to enlarge.

Klein and Hartmann (1993) showed that there is a close relation of monthly average low cloud fractional coverage to the 'low tropospheric stability', defined as the difference between 700 mb temperature and SST. This gives the possibility of a positive feedback

Colder SST  $\rightarrow$  stronger stability of the low troposphere  $\rightarrow$  more stratus

## Simulated Stratus Cloud and Surface Wind Stress

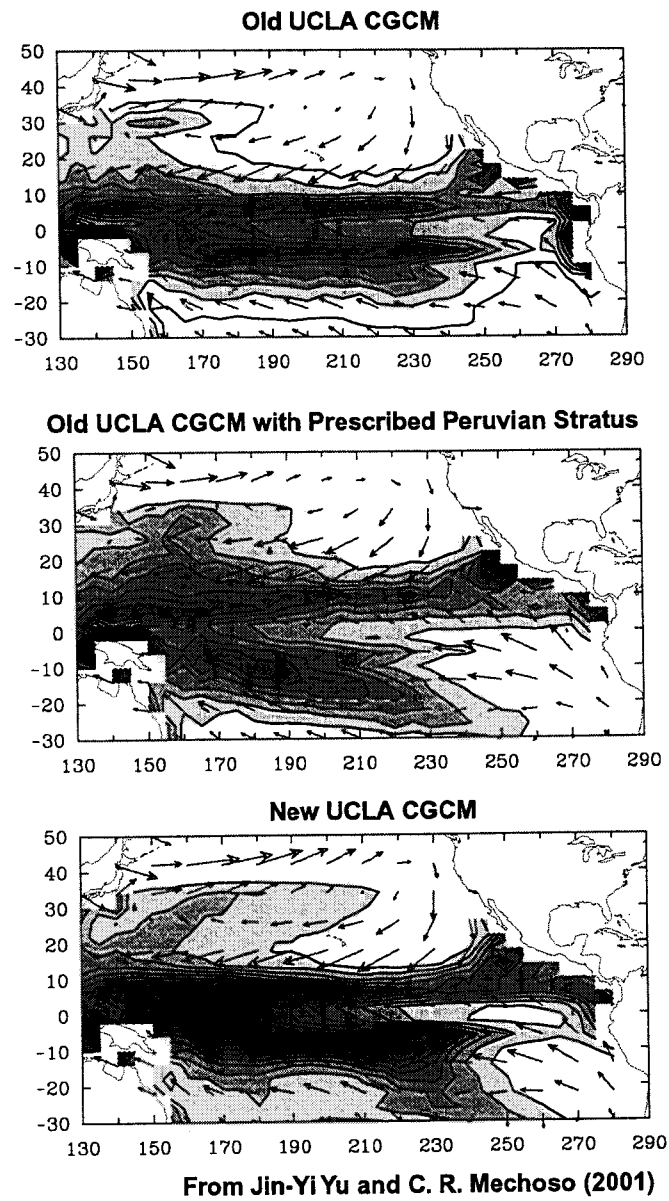


Figure 2. Stratus cloud sensitivities in the UCLA coupled GCM..

# **Coupled Stability Analysis**

## **Linearization of Coupled System :**

1. Forward Deterministic Approach
2. Inverse Statistical Approach

## **Normal Mode Analysis :**

1. Coupled Instability
2. Important Parameters
3. Classification of Coupled Modes

## **Singular Vector Analysis :**

1. Nonnormal Growth
2. Optimal Initial Conditions

# Linearization

## Forward Technique :

1. Start from a set of deterministic equations based on 1st principle.

$$\frac{\partial s_a}{\partial t} = f(s_a, sst), \quad (1)$$

$$\frac{\partial s_o}{\partial t} = g(s_o, \tau), \quad (2)$$

where

- $s_a$ : state vector of atmospheric variables,
- $sst$ : sea-surface temperature,
- $s_o$ : state vector of oceanic variables,
- $\tau$ : atmospheric fluxes at sea surface.

2. Linearize equations of motion about a mean climatic state. Define anomalies,  $s'_o = s_o - \bar{s}_o$  and  $s'_a = s_a - \bar{s}_a$ :

$$\frac{\partial s'_a}{\partial t} = \frac{\partial f}{\partial s_a} \Big|_{\bar{s}_a} s'_a + \frac{\partial f}{\partial sst} \Big|_{\bar{sst}} sst' + N_a, \quad (3)$$

$$\frac{\partial s'_o}{\partial t} = \frac{\partial g}{\partial s_o} \Big|_{\bar{s}_o} s'_o + \frac{\partial g}{\partial \tau} \Big|_{\bar{\tau}} \tau' + N_o. \quad (4)$$

## Linear Coupled Model

**Assumption** : Atmosphere has a fast adjustment time scale, so that its variability can be divided into a quasi-equilibrium response to SST and a quasi-random part due to nonlinear processes.

Set  $\frac{\partial s'_a}{\partial t} = 0, \Rightarrow \tau' = Csst' + N_a$ ; **C** a coupling matrix.

**Linear Coupled Model** :

$$\frac{\partial s'_o}{\partial t} = As'_o + N. \quad (5)$$

where

- **A**: System matrix or dynamic operator,
- **N**: Uncoupled atmos. and oceanic processes.

**Useful Parameters** : Two important time scales:

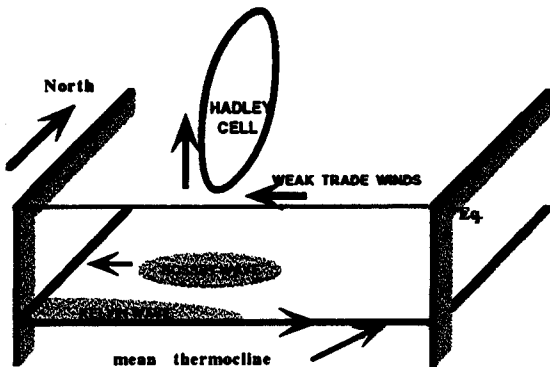
$T_c \sim$  time scale associated with air-sea feedback,

$T_o \sim$  time scale associated with oceanic adjustment,

$R = \frac{T_o}{T_c}$  measures relative importance.

# Regime Diagram of the Tropical Ocean-Atmosphere System

$$R = \frac{\text{atmospheric coupling}}{\text{ocean adjustment}} = \frac{T_0}{T_c}$$

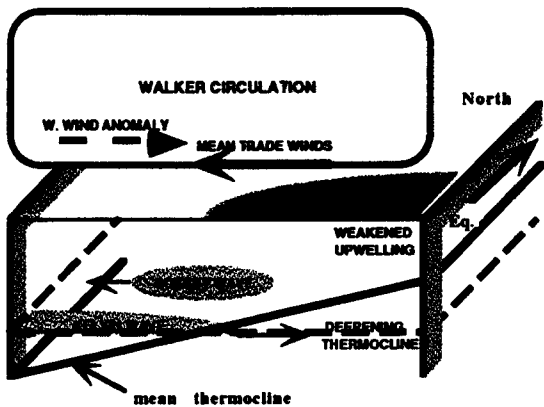


## Weakly Coupled Atm & Ocean

- Free Kelvin & Rossby waves
- Discrete ocean basin modes with the lowest frequency of 9-mos.

$R \ll 1$

(Pre-TOGA)

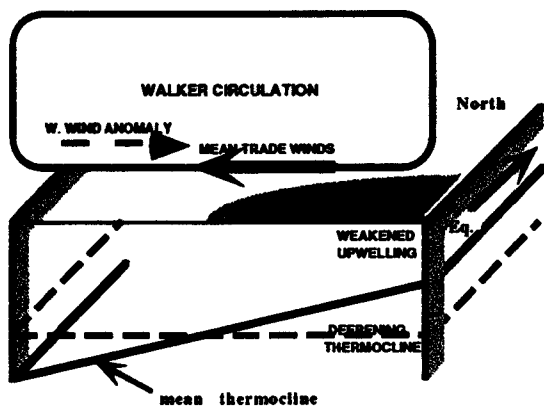


## Realistic Atm. & Ocean Coupling

- Air-sea feedback  $\leftrightarrow$  ocean adjust.
- Subsurface oceanic memory is important
- Mixed SST/ocean dynamics coupled modes  $\rightarrow$  the delayed oscillator mode.

$R = O(1)$

(TOGA)



## Strongly Coupled Atm. & Ocean

- Bjerknes feedback dominates coupled dynamics
- Strong growing stationary coupled modes (non-oscillatory)

$R \gg 1$

(Pre-TOGA)

**There are two important processes in the tropical coupled system -- air-sea feedback and ocean adjustment. Dynamics of the tropical coupled system depends on a parameter  $R$  which measures the relative importance of these two processes:**

**If coupling is weak  $R \ll 1$ , then oceanic waves are not influenced by the air-sea coupling. Therefore, there exist free equatorially trapped waves and superposition of these waves gives rise to discrete ocean basin modes with the lowest frequency of 9-mos.**

**In the other limit where coupling is very strong ( $R \gg 1$ ), then the coupled system supports only strong growing stationary coupled modes. These modes are non-oscillatory and thus the coupled system has no preferred frequency.**

**The most interesting and also most complicated regime is when air-sea feedback is comparable to ocean wave adjustment. In this case, there is a family of coupled modes called mixed SST/ocean dynamics modes (Neelin and Jin). Depending on which oceanic processes dominate SST changes, the modes can be either stable or unstable, propagating or stationary, and can have various period. Among them, the mode that is believed to be most relevant to the reality is the delayed oscillator mode.**

# Coupled Stability Analysis

**Coupled Mode** : Eigen decomposition of  $\mathbf{A}$ ,  $\mathbf{A} = \mathbf{E}\mathbf{\Lambda}\mathbf{E}^{-1}$ , gives a spectrum of eigenvalues  $\mathbf{\Lambda}$  and eigenvectors  $\mathbf{E}$ . These are the coupled modes.

$e^{\lambda t}$

**Unstable Mode** : Those coupled modes with  $Re(\lambda) > 0$  are unstable modes. The most unstable mode dominates the evolution of the system as  $t \rightarrow \infty$ .

## Classification of Modes :

- **SST-Mode**: Ekman feedback and SST advection dominate; subsurface adjustment is not important.
- **Ocean-Dynamics Mode**: In the limit of weak coupling; the low-frequency ocean basin mode has a period of 9-10 months.
- **Mixed SST-Ocean-Dynamics Mode**: Air-sea feedback and subsurface ocean adjustment time scales are comparable.

## An Example: Cane-Zebiak Model

**Ocean** :  $1\frac{1}{2}$ -layer ocean with an embedded mixed layer:

$$(\delta\partial_t + \epsilon_m)u'_m - yv'_m + \partial_x h' = \tau', \quad (6)$$

$$yu'_m + \partial_y h' = 0, \quad (7)$$

$$(\delta\partial_t + \epsilon_m)h' + \partial_x u'_m + \partial_y v'_m = 0, \quad (8)$$

$$\epsilon_s u'_s - yv'_s = \delta_s \tau', \quad (9)$$

$$\epsilon_s v'_s + yu'_s = 0, \quad (10)$$

$$\partial_t T + \mathbf{v}\nabla T + \frac{w(T - T_{sub})}{D} + \epsilon_T(T - T_0) = 0. \quad (11)$$

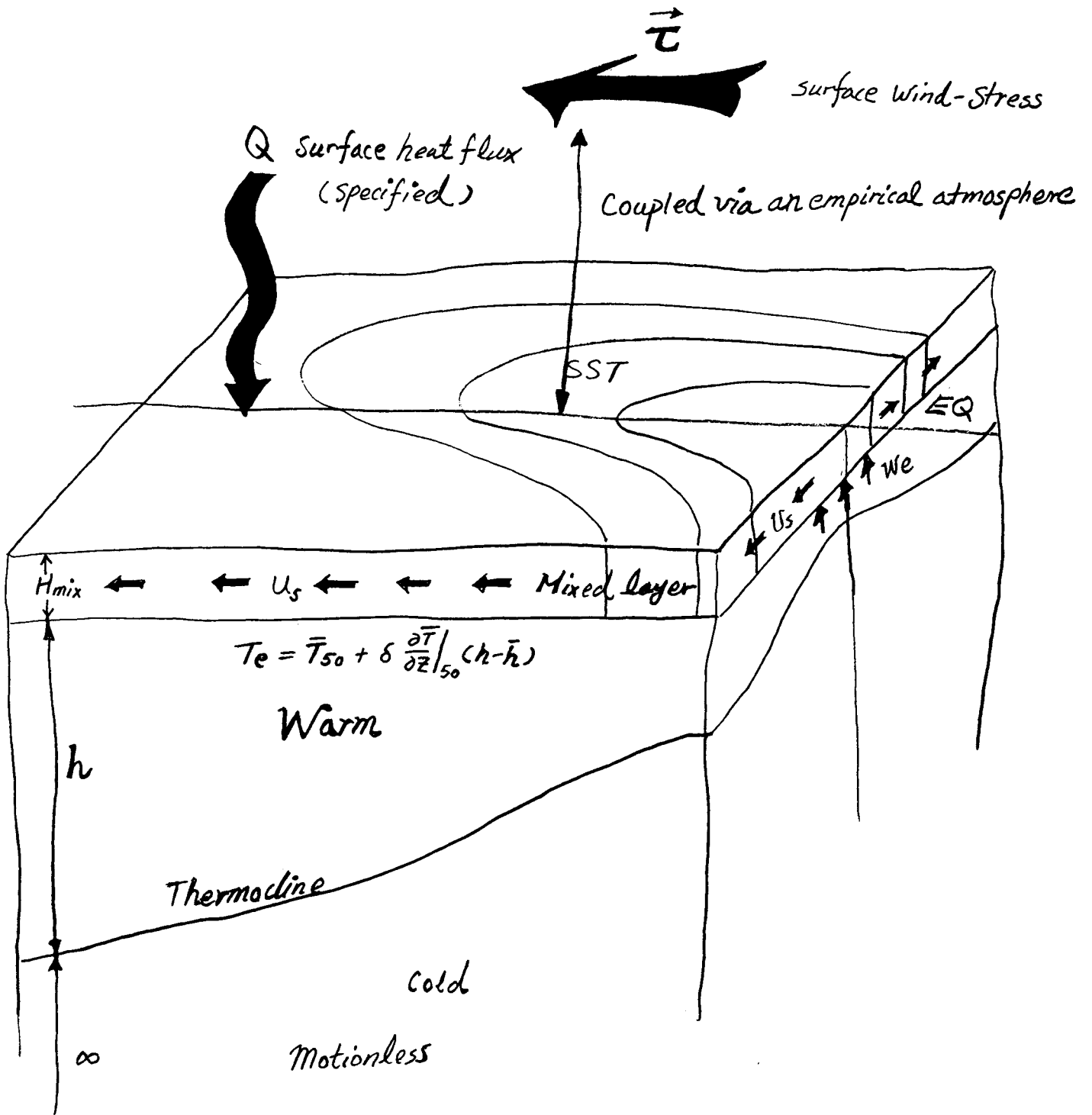
**Atmosphere** : Gill type atmosphere:

$$\tau' = \mu C T', \quad (12)$$

where

- $\delta$ : oceanic adjustment time parameter,
- $\mu$ : air-sea coupling parameter,
- $\delta_s$ : Ekman feedback parameter.

# A Schematic of Coupled Model



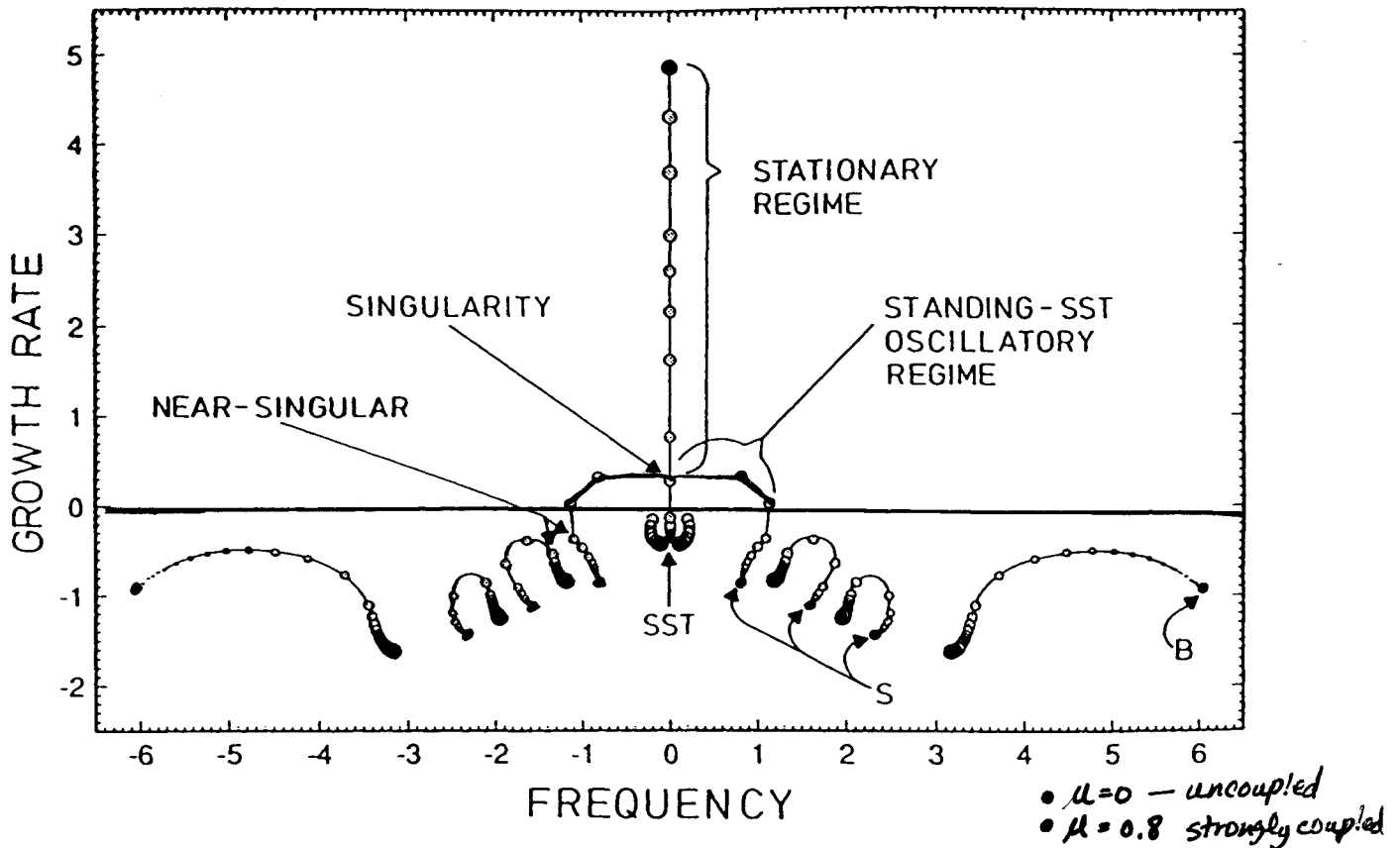


Figure 7 Eigenvalues of the five leading modes of the Jin & Neelin (1993a) intermediate coupled model as a function of coupling coefficient,  $\mu$ , for a realistic value of the relative time scale coefficient,  $\delta = 1.5$ . Dots give frequency and growth rate of each mode on the complex plane, with dot size representing coupling for constant increments from  $\mu = 0$  to  $\mu = 0.8$ . Eigenvalues trace out continuous paths as a function of coupling (indicated by interpolated lines for clarity). Uncoupled modes (ocean basin mode *B*, discretized scattering modes *S*, and an SST mode) are indicated at  $\mu = 0$  (smallest dots). The modes have mixed character for larger  $\mu$ : The purely growing mode which produces the *stationary regime*, indicated over the range of large  $\mu$ , is closely related to the stationary SST mode; this is connected at a singularity to the important *standing-SST oscillatory regime* which extends over a range of moderate coupling values.

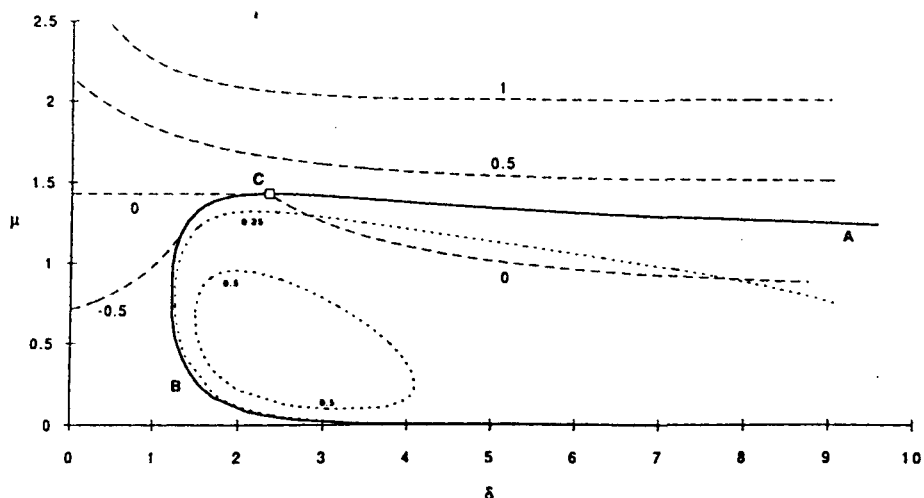


Figure 9. Dispersion relation of the SSBH delayed oscillator model as a function of coupling coefficient  $\mu$  and relative timescale coefficient  $\delta$ . Long dashed lines are contours of growth rate; short dashed lines are contours of frequency (nondimensional). The solid line indicates the transition between regions where the mode is oscillatory or purely growing/decaying. The transition to pure growth behavior along C to A corresponds to behavior found in ICMs. The transition along the curve marked B does not correspond to ICM behavior and is an artifact of approximations to ocean dynamics.

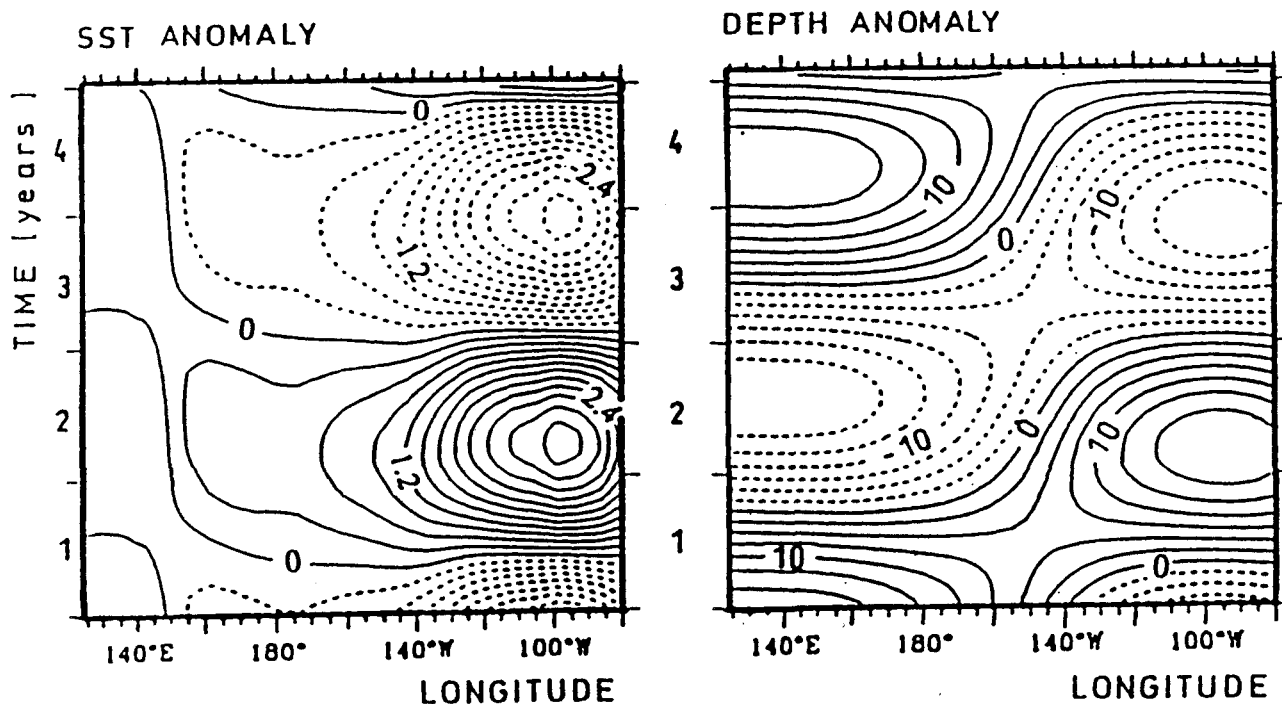


Figure 10. SST and thermocline depth anomalies from the linearized version of the CZ model of Battisti and Hirst [1989] over one period of the simulated ENSO cycle. After Battisti and Hirst [1989].

# Prototype ENSO Models

**Delayed Oscillator** : Wave adjustment  $\Rightarrow$  a delay  $4\delta$ :

$$\frac{dT'}{dt} + [T' - T'_{sub}(h')] = 0, \quad (13)$$

$$h'(t) = \mu[b_0T'(t) - b_1T'(t - 4\delta)]. \quad (14)$$

where

- $T'$ : averaged SST anomaly in the east,
- $T'_{sub}$ : subsurface temperature in the east,
- $h'$ : thermocline depth in the east.

**Recharged Oscillator** : N-S mass flux  $\Rightarrow h'_w$ :

$$h'_e = h'_w + \tau', \quad (15)$$

$$\delta \frac{dh'_w}{dt} = rh'_w - \alpha\tau', \quad (16)$$

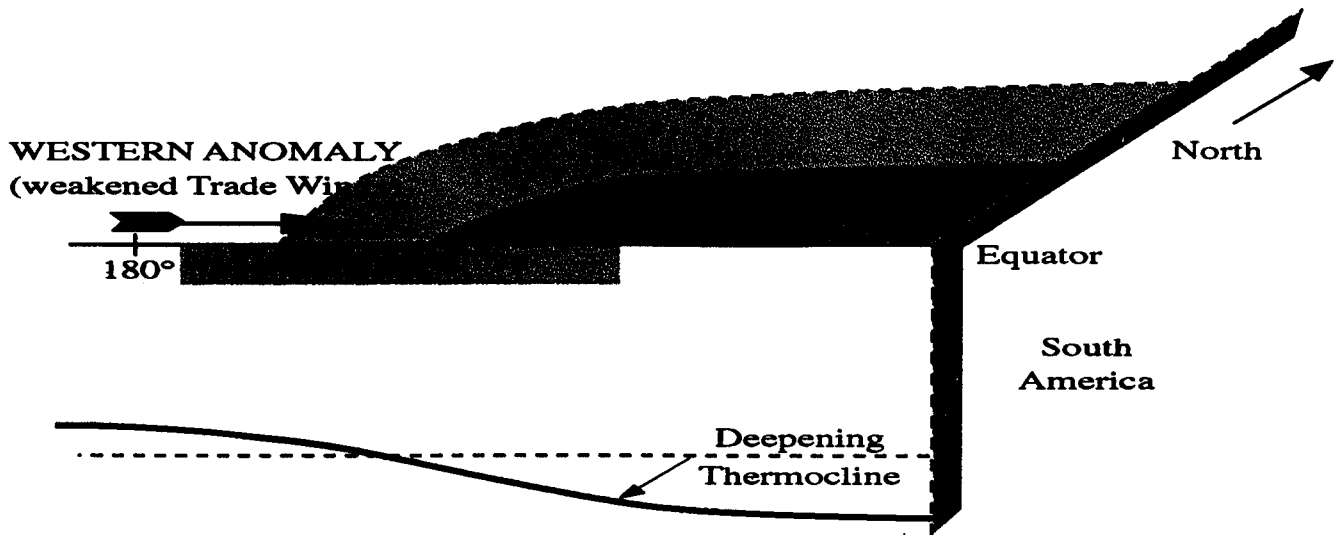
$$\frac{dT'}{dt} = -cT' + \gamma h'_e + \delta_s \tau', \quad (17)$$

$$\tau' = \mu T' \quad (18)$$

where

- $h'_w$ : thermocline depth at the west,
- $h'_e$ : thermocline depth at the east,
- $T'$ : averaged SST anomaly in the eastern Pacific.

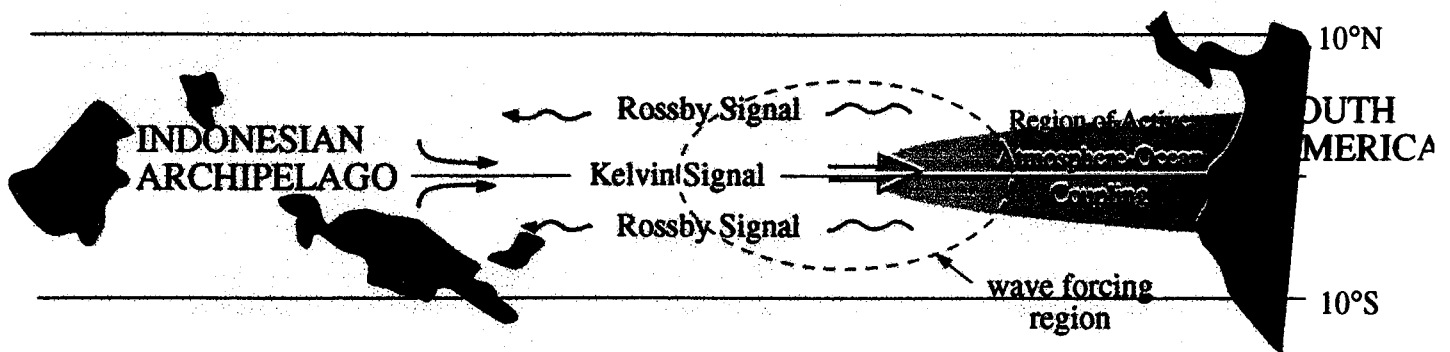
# ENSO Delayed Oscillator Model



Bjerknes air-sea feedback

$$dT/dt = b T(t) - c T(t-\tau)$$

Ocean Wave Adjustment



The delayed oscillator model offers an explanation for the turnabout between warm and cold phase of the ENSO cycle. The period of ENSO is determined by a competition between the Bjerknes positive air-sea feedback and the negative feedback due to subsurface ocean adjustment. The theory points to the importance of subsurface ocean memory, particularly in the western Pacific Ocean.

**The delayed oscillator consists of two parts -- the Bjerknes air-sea feedback part and ocean wave adjustment part. The air-sea feedback amplifies a warm SST perturbation by reducing upwelling and deepening the thermocline due to a relaxation in the trades. Meanwhile, the westerly winds also introduce upwelling Rossby wave off the equator, which turn into an upwelling Kelvin wave after a certain delay (5-6 mos). The upwelling Kelvin wave off sets the warming the eastern equatorial Pacific by bring the cold subsurface water into the surface layer. It is this delayed wave adjustment that makes the ENSO oscillate. Using realistic parameters, the delayed oscillator has period between 3-4 years.**

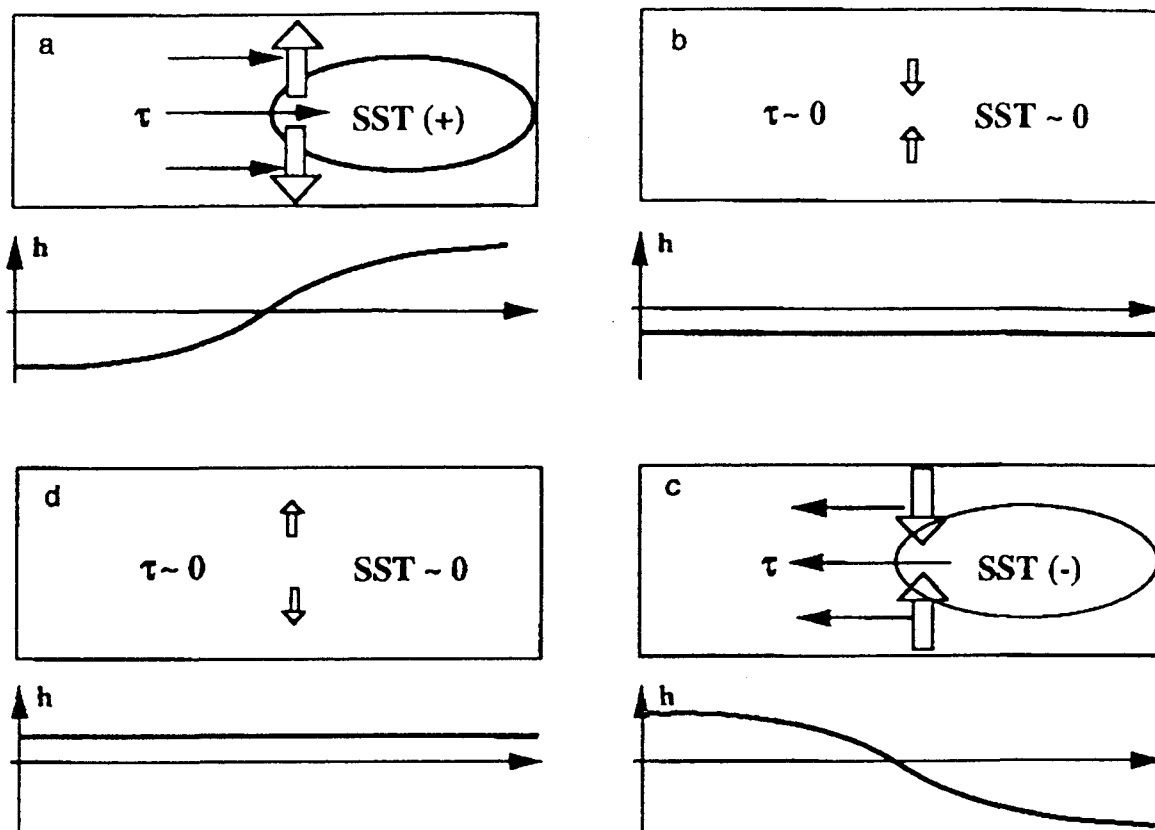


FIG. 1. Schematic panels of the four phases of the recharge oscillation: (a) the warm phase, (b) the warm to cold transition phase, (c) the cold phase, and (d) the cold to warm transition phase. The rectangular box represents the equatorial Pacific basin, the elliptical circle represents the SST anomaly, the thin and filled arrows represent wind stress anomaly associated with the SST anomaly, and the thick unfilled arrows represent the recharge/discharge of equatorial heat content. Each panel also shows the distribution of the thermocline depth anomaly ( $h$ ) along the equator.

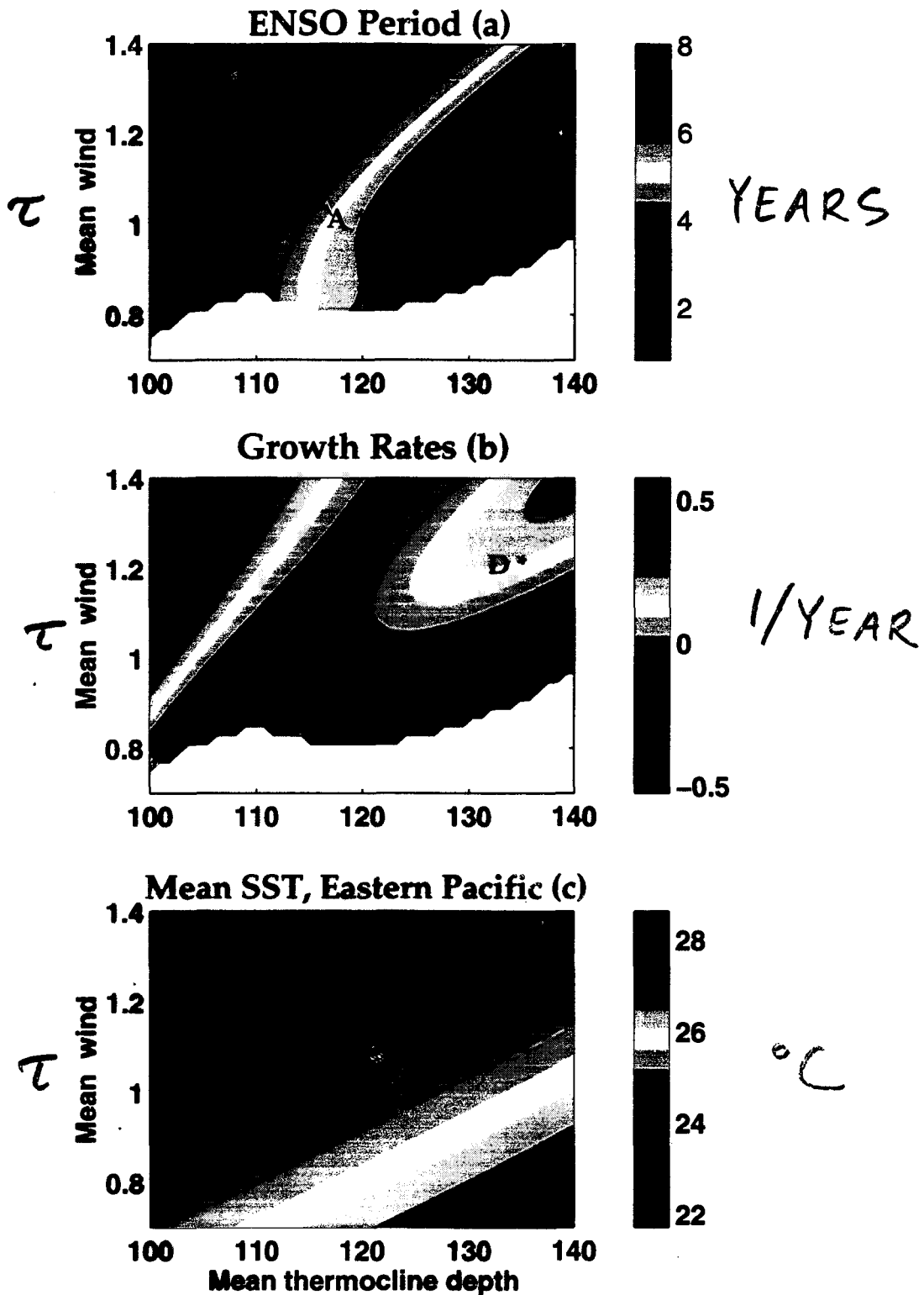
## Dependence on Mean States

### Mean State Parameters :

- $H$ : Mean thermocline depth,
- $\tau$ : Mean zonal winds,
- $\Delta T$ : Mean vert. temperature gradient.

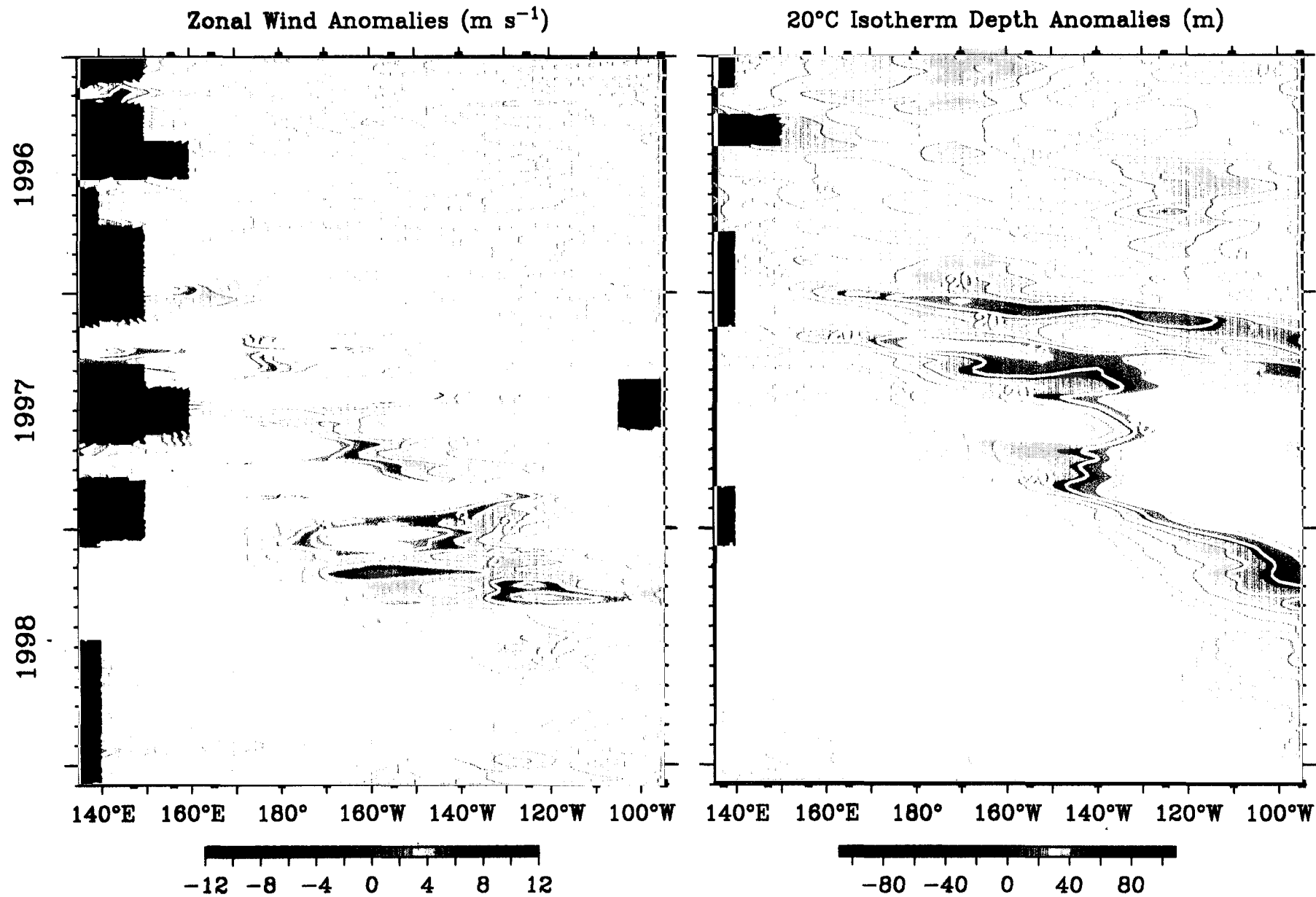
**Delayed Oscillator (Remote) Mode** :  $H$  is deep and  $\tau$  is strong so that the west-to-east thermocline slope is large. The temperature change is dominated by vertical movement of the thermocline  $\bar{W} \partial_z T'$ .

**SST (local) Mode** :  $H$  is shallow and  $\tau$  is strong so that the temperature gradients are large. The temperature change is dominated by the advection by anomalous current  $u' \partial_x \bar{T} + w' \partial_z \bar{T}$ . The thermocline effect is small.



The period (a) and growth rates (b) of the most unstable oscillations as a function of changes in the easterly winds along the equator, and the depth of the equatorial thermocline (in meters); SST of the mean state in the Eastern Pacific (c).

# Five-Day Zonal Wind and 20°C Isotherm Depth 2°S to 2°N Average



## Linear Inverse Model

**Assumption** : Coupled system is stable  $\Leftrightarrow \lambda(\mathbf{A}) < 0$ :

$$\frac{\partial s'_o}{\partial t} = \mathbf{A}s'_o + N, \quad (19)$$

where  $N$ : a spatially coherent white noise.

**Estimate Propagator** : Solution to LSM:

$$s'_o(t + \Delta t) = e^{(\mathbf{A}\Delta t)}s'_o(t) + N' \quad (20)$$

where  $e^{(\mathbf{A}\Delta t)}$ : propagator. Given a multivariate time series  $s'_o(t)$ ,  $e^{(\mathbf{A}\Delta t)}$  can be estimated by

$$e^{(\mathbf{A}\Delta t)} = \mathbf{C}_{\Delta t}\mathbf{C}_0^{-1}, \quad (21)$$

where

- $\mathbf{C}_{\Delta t} = \langle s'_o(t + \Delta t)s'^T_o(t) \rangle$ : lag-covariance matrix,
- $\mathbf{C}_0 = \langle s'_o(t)s'^T_o(t) \rangle$ : covariance matrix.

**POP Analysis** : Eigen-decomposition of  $e^{(\mathbf{A}\Delta t)}$ :

$$e^{(\mathbf{A}\Delta t)} = \mathbf{E}\hat{\mathbf{\Lambda}}\mathbf{E}^{-1}; \quad (22)$$

$$\mathbf{A} = \mathbf{E}\log(\hat{\mathbf{\Lambda}}/\Delta t)\mathbf{E}^{-1} \quad (23)$$

where

- $\mathbf{E}$ : normal modes of  $\mathbf{A} \Rightarrow$  Coupled Modes,
- $\log(\hat{\mathbf{\Lambda}}/\Delta t)$ : eigenvalues of  $\mathbf{A} \Rightarrow$  Damping, Period.

## Singular Vector Analysis

**Nonnormal Growth** : Even when the coupled system is stable,  $\lambda(\mathbf{A}) < 0$ , variance of  $s'_o(t + \Delta t)$  can grow reference to its initial variance. This nonnormal mode growth is due to the interference among the non-orthogonal normal modes and can be determined by Singular Value Decomposition (SVD) of the propagator  $e^{(\mathbf{A}\Delta t)}$ :

$$e^{(\mathbf{A}\Delta t)} = \mathbf{U}\mathbf{\Sigma}\mathbf{V}^T, \quad (24)$$

$$\mathbf{U}\mathbf{U}^T = \mathbf{I} \quad \text{and} \quad \mathbf{V}\mathbf{V}^T = \mathbf{I}. \quad (25)$$

**Optimal Initial Condition** : Take initial condition  $s'_o(t)$  be the first vector of  $\mathbf{V}$ ,  $v_1$ , which has the largest singular value  $\sigma_1$ , variance of  $s'_o(t + \Delta t)$  has the maximum growth,

$$s'_o(t + \Delta t) = \sigma_1 u_1, \quad (26)$$

$$\frac{\text{var}(s'_o(t + \Delta t))}{\text{var}(s'_o(t))} = \sigma_1^2. \quad (27)$$

where

- $v_1$ : Optimal initial condition,
- $u_1$ : Maximum response pattern,
- $\sigma_1^2$ : maximum variance growth.

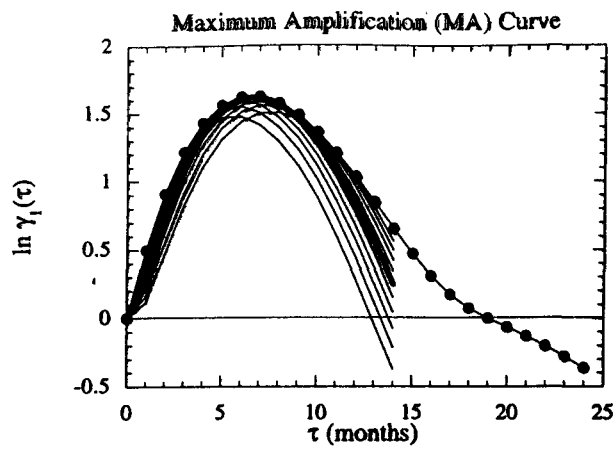
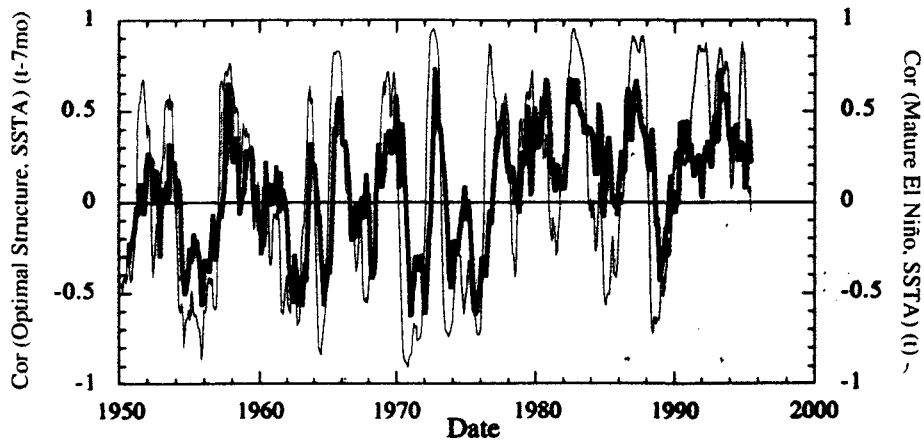
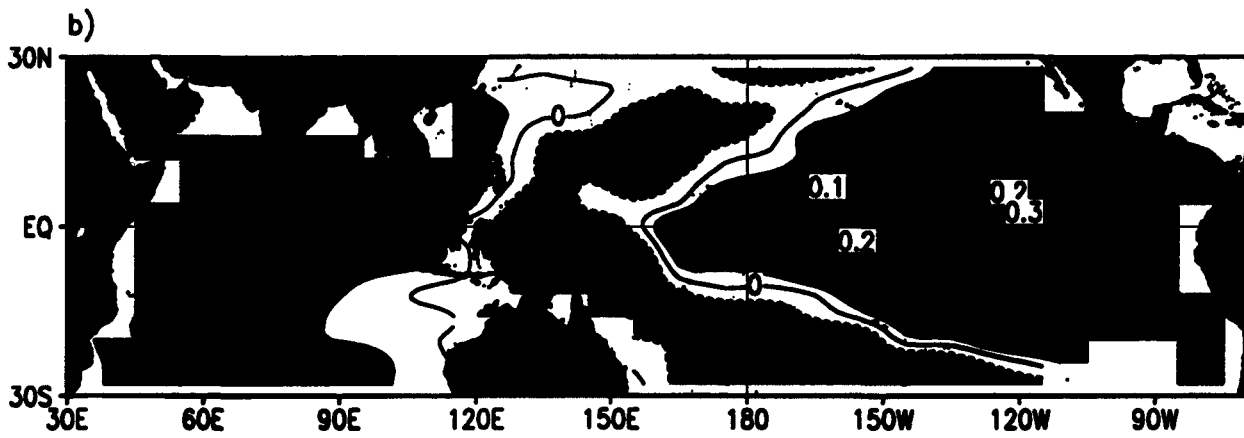
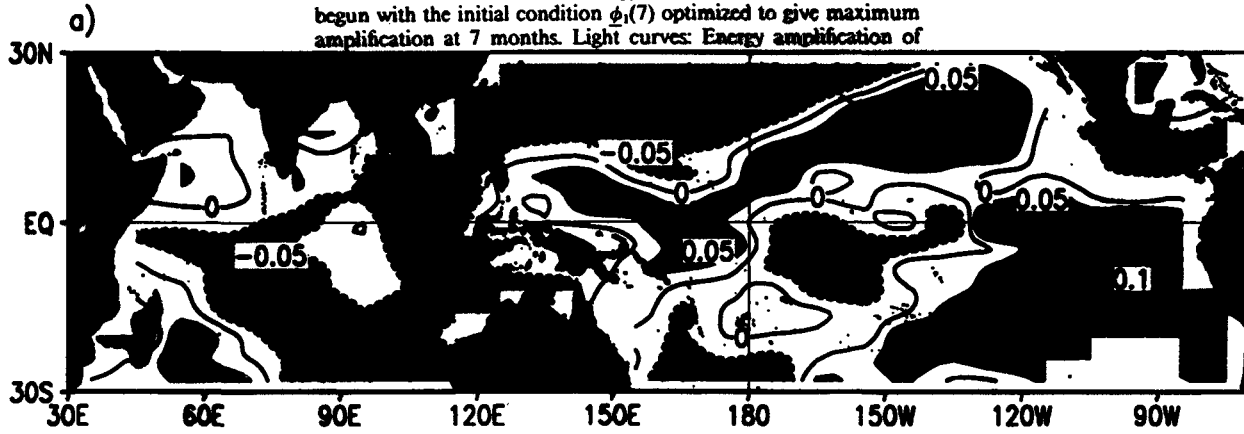


FIG. 4. (a) Thick curve with filled circles: The maximum amplification curve. Thick curve: Energy amplification of a forecast (6) begun with the initial condition  $\phi_1(7)$  optimized to give maximum amplification at 7 months. Light curves: Energy amplification of



MONTHLY WEATHER REVIEW

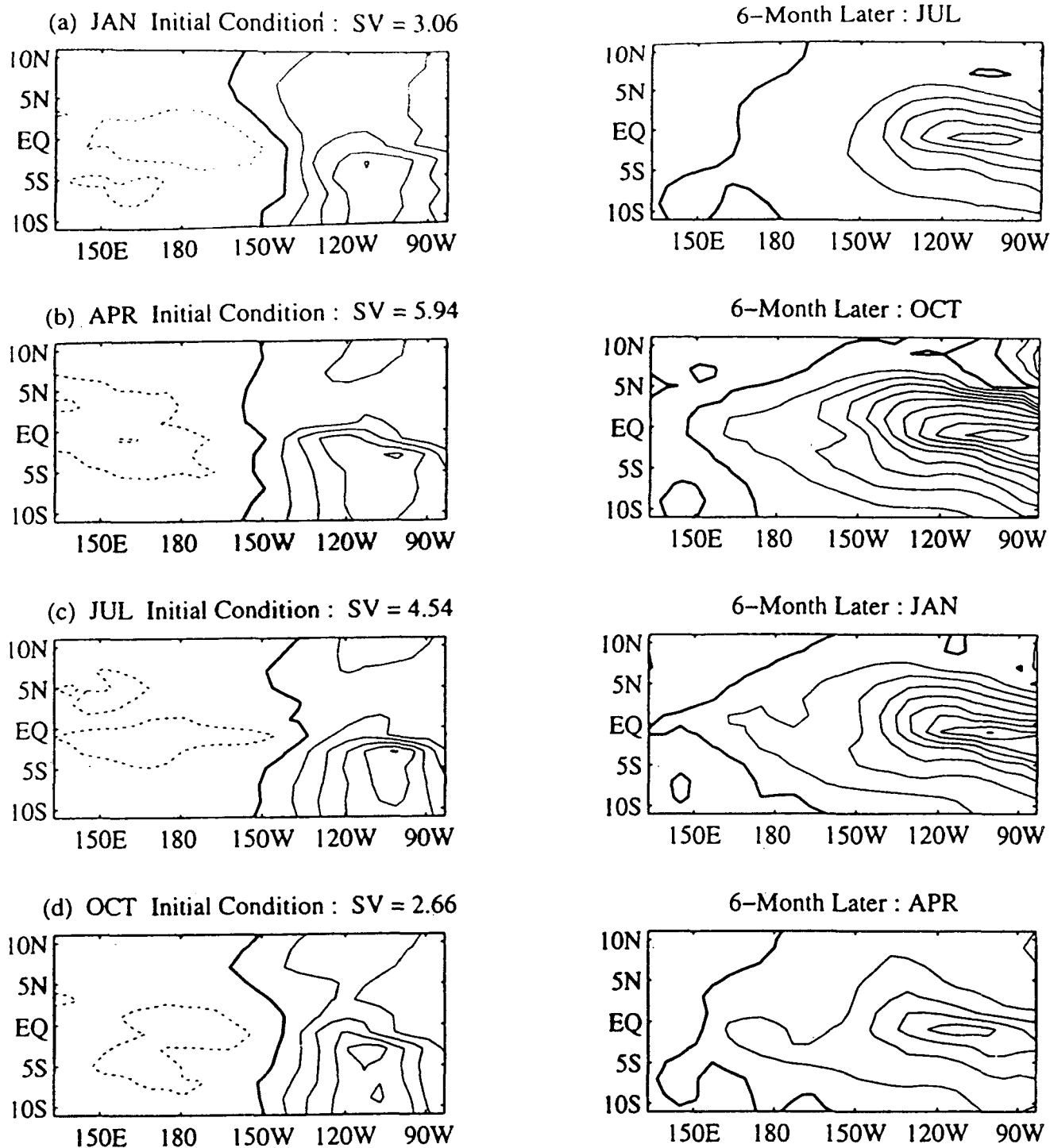


FIG. 2. (a) The optimal SST perturbation applied in January (left) that produces the maximum amplitude in SST six months later in July (right). Panels (b), (c), and (d) are for optimal perturbations applied in April, July, and October, respectively. The contour interval for the initial (final) perturbations in the left (right) column is  $0.04^{\circ}\text{C}$  ( $0.12^{\circ}\text{C}$ ). For each case,  $\lambda_1$  is noted above the left panel.

# Linear Stochastic ENSO Theory

## Assumptions :

1. The ENSO system is stable, so that ENSO evolution is not dominated by a single normal mode.
2. The internal variability of the atmosphere acts as an external (spatially coherent) white-noise forcing to maintain ENSO variability.

## How Does It Work ?

1. A group of damped normal modes interferes constructively or destructively, depending on their excitation by the stochastic forcing, to give SST growth or decay.

## What Does the Theory Predict ?

1. Broad band spectrum.
2. The existence of optimal initial condition and optimal stochastic forcing.

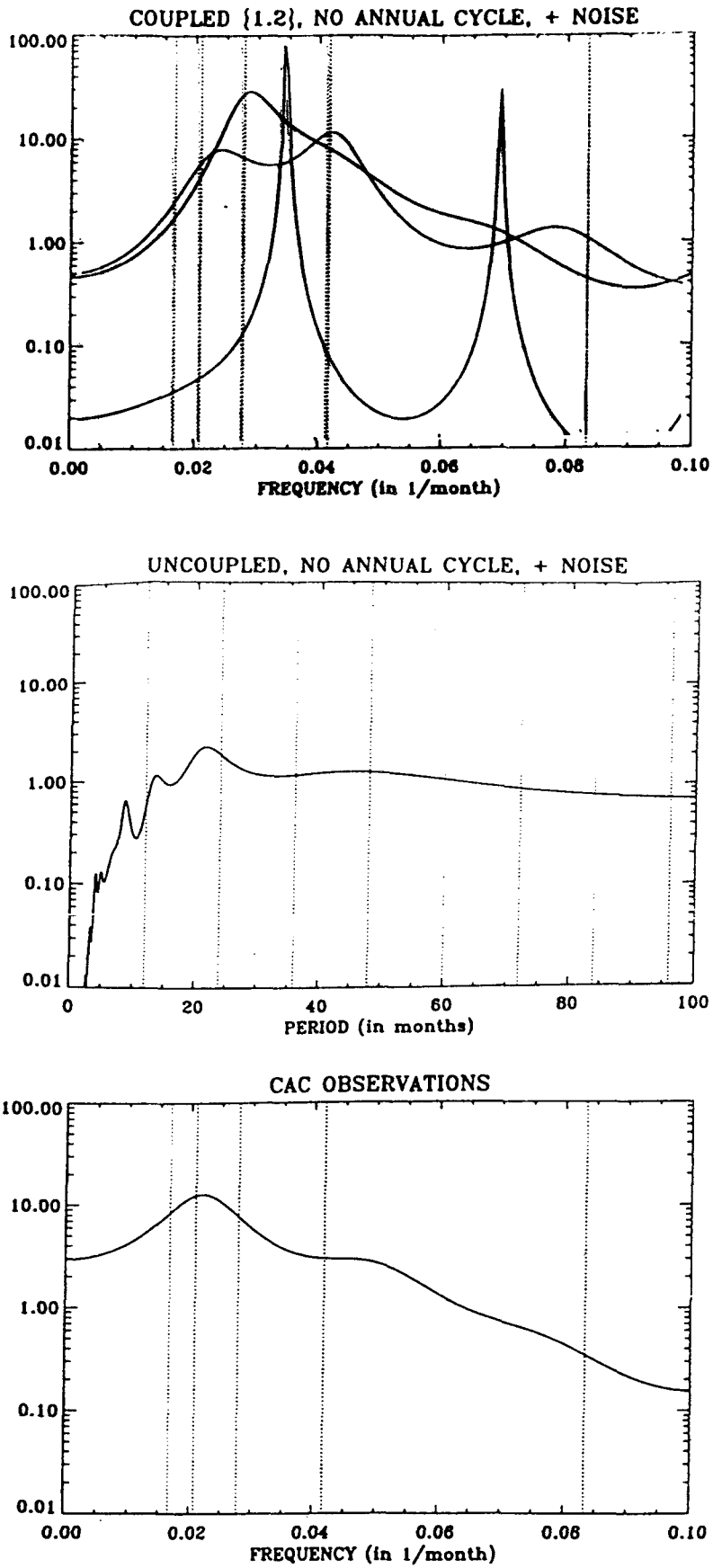


FIG. 4. Power spectrum of the Niño3 SST anomaly time series: (a) as a function of the period, for a 112-yr simulation with the OGCM only (uncoupled mode) forced by the empirically estimated stochastic wind stress product added to the mean annual observed stress; (b) as a function of the frequency, for the observations (period 1950–93). Spectra from the maximum entropy method (MEM) of order 30.

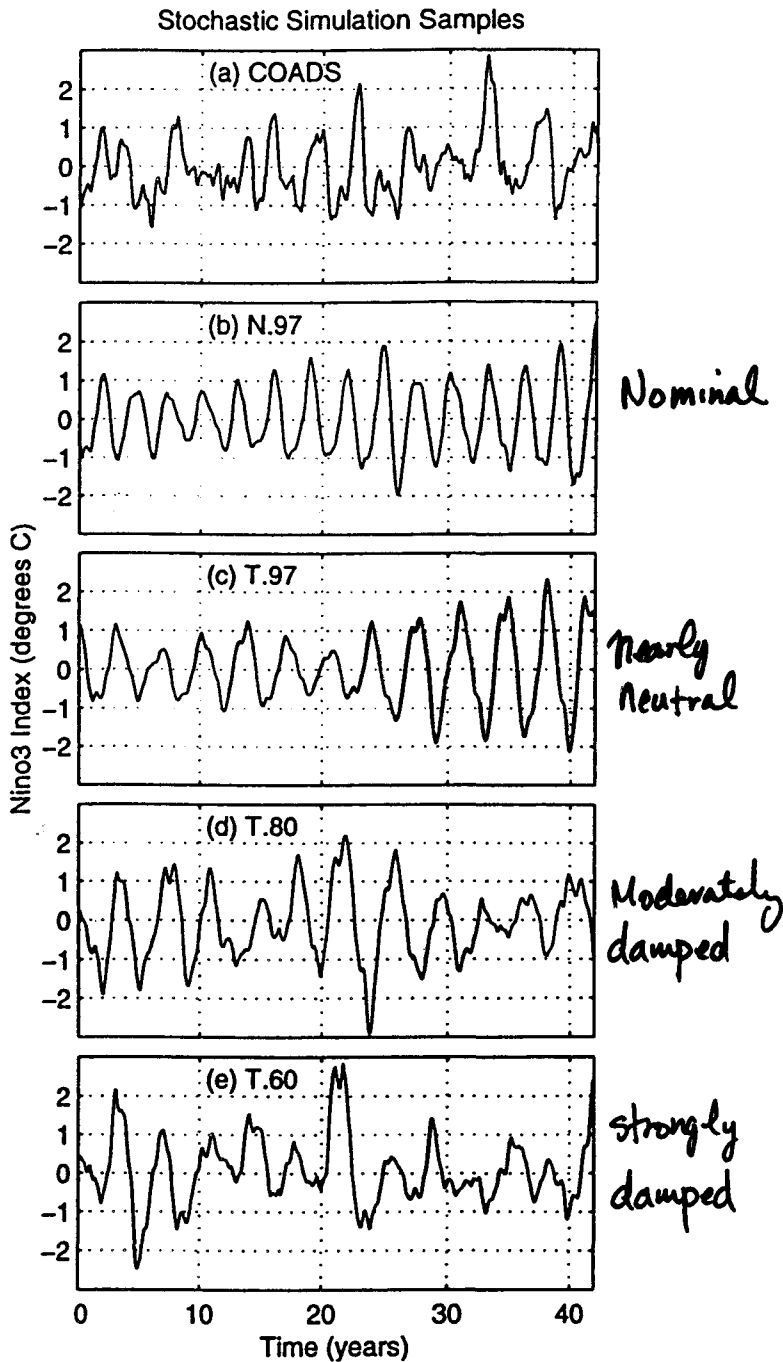


FIG 13. Niño3 index from the COADS data and a 42 year sample from the stochastic simulations of each of the candidate models.

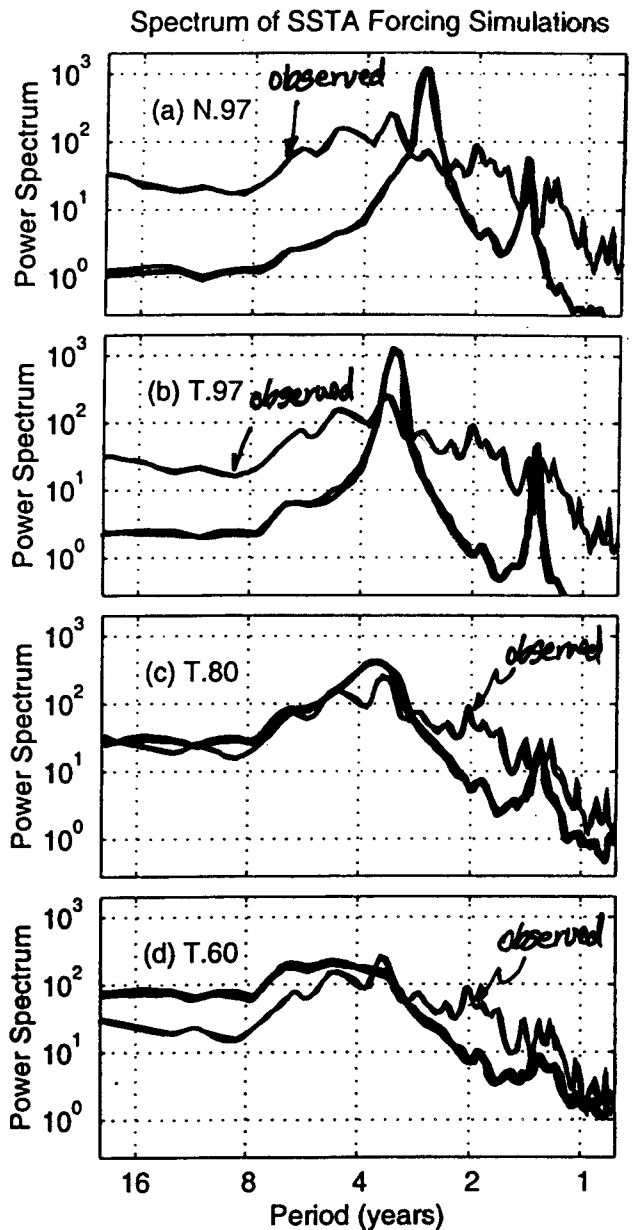


Figure 4. Power Spectra of Candidate Models. The thick lines in panels (a) through (d) show the spectrum of the Niño3 index for the N.97, T.97, T.80, and T.60, respectively. The thin line repeated in all four panels shows the COADS spectrum for comparison.

Pealand, Flügel and Chang (1999) Global Error Variance  $\langle \tilde{e}^* \tilde{e} \rangle$

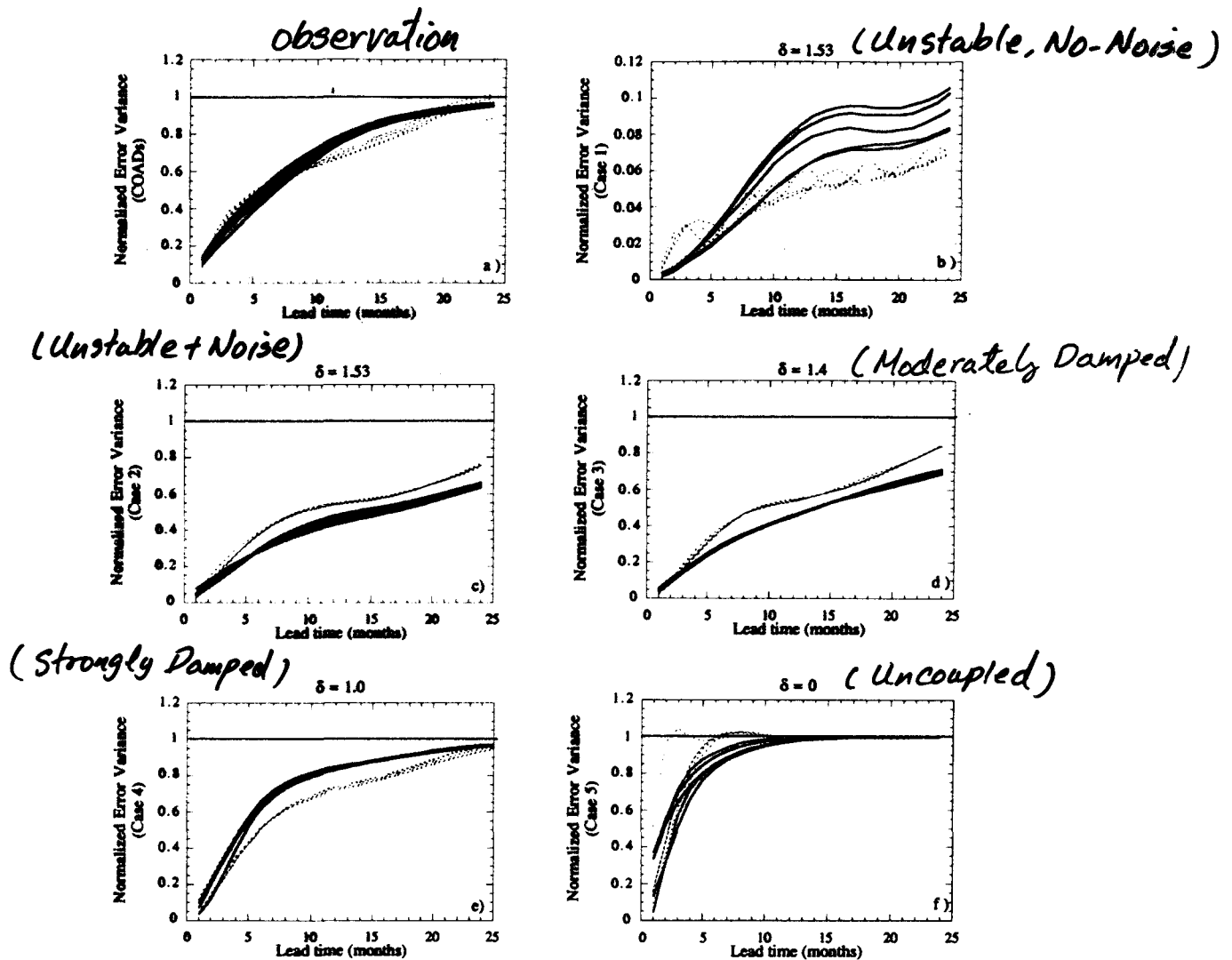


Fig.3) Normalized error variance as a function of lead time. Solid lines: Theoretically-expected error curves for  $\tau_0 = 3, 4, 5, 6, 7$  months. Dotted lines: Corresponding observed error curves. a) COADS data as analyzed by PS95. b-f) Error curves for Cases 1 through 5, respectively.

## Predictability Analysis

Given a multivariate linear stochastic system,

$$\frac{d\vec{\theta}}{dt} = \mathbf{A}\vec{\theta} + \mathbf{F}\vec{\eta}, \quad (1)$$

the optimal forecast model under the “perfect initial condition scenario” is

$$\vec{\theta}_s(\tau; t_0) = e^{\mathbf{A}\tau}\vec{\theta}_0(t_0) \quad (2)$$

with

$$\vec{\theta}_0(t_0) = \int_0^{t_0} e^{\mathbf{A}(t_0-s)}\mathbf{F}\vec{\eta}_0(s)ds$$

where  $\tau = t - t_0$  is called lead time of the prediction. Prediction error is

$$\vec{\theta}_e = \int_{t_0}^t e^{\mathbf{A}(t-s)}\mathbf{F}\vec{\eta}(s)ds. \quad (3)$$

The normalized error error variance

$$\epsilon^2(\tau) = \frac{\sigma_e^2(\tau)}{\sigma_\infty^2} = \frac{tr(\mathbf{C}(\tau))}{tr(\mathbf{C}(\infty))} \quad (4)$$

gives a predictability measure, where  $\mathbf{C}(\tau)$  and  $\mathbf{C}(\infty)$  are error and climatological covariance matrices.

# System Dynamics $\Leftrightarrow$ Predictability

**Dynamic Operator  $A \Leftrightarrow$  Predictability:** Given noise  $F$ , e.g., a unitary noise  $FF^{-1} = I$ ,  $\epsilon^2$  depends only on the characteristics of the normal modes, i.e.,  $E$  and  $\Lambda$ . Two important results emerge:

1. For  $EE^{-1} = I$ , i.e.,  $A$  is normal,  $\epsilon^2$  depends only on  $Re(\Lambda)$ . Predictability is independent of oscillation period.
2.  $\epsilon^2$  of a normal system grows fastest, implying the least predictability.

**Noise Forcing  $F \Leftrightarrow$  Predictability:** Given system dynamics  $A$ ,  $\epsilon^2$  depends only on spatial structure of noise forcing  $A$ . There exists an optimal forcing  $\vec{f}$  that minimizes  $\epsilon^2$  or maximizes predictability. The optimal forcing  $\vec{f}$  is completely determined by the propagator and is the eigenvector of  $B(\infty)\vec{f} = \nu B(\tau)\vec{f}$ , where  $B(\tau) = \int_0^\tau e^{A^*s}e^{As}ds$ .  $\vec{f}$  degenerates to the so-called "stochastic optimal" at very short lead times.

**Predictable Component Analysis:** Given  $A$  and  $F$ ,  $C(\infty)C(\tau)^{-1}\vec{p} = \nu\vec{p}$  gives the most predictable pattern  $\vec{p}$  that minimizes  $\epsilon^2$ .

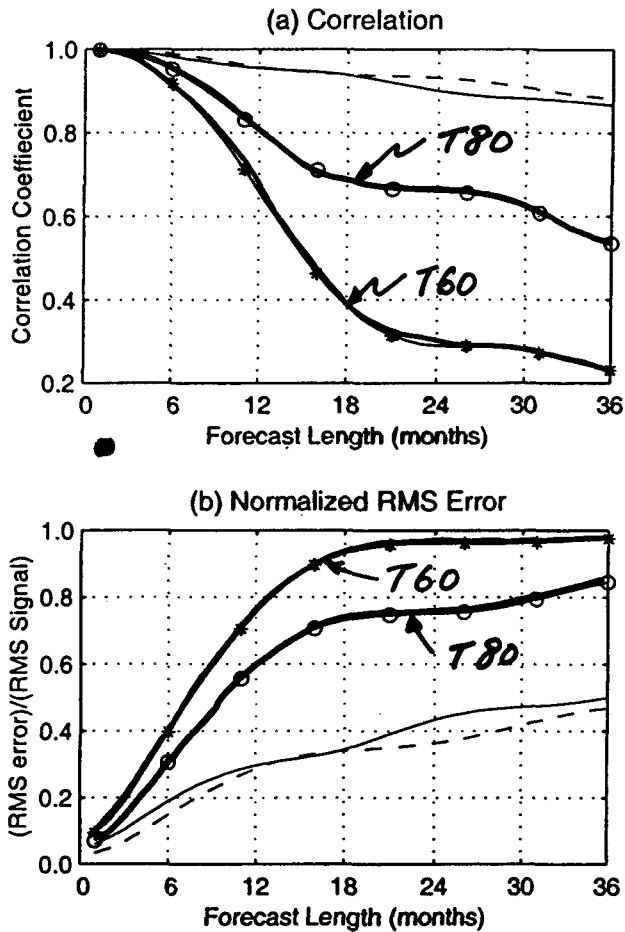


Figure 13. Averaged Potential Predictability Limit. Panel (a) shows the correlation of the Nino3 index from a simulation with the Nino3 index which is forecast using the same model with perfect initialization, but without knowledge of future noise forcing. Panel (b) shows the average normalized RMS error for the same forecasts. The key for both panels is as follows: the solid line is N.97; the dashed line is T.97; the circles are T.80; the asterisks are T.60.

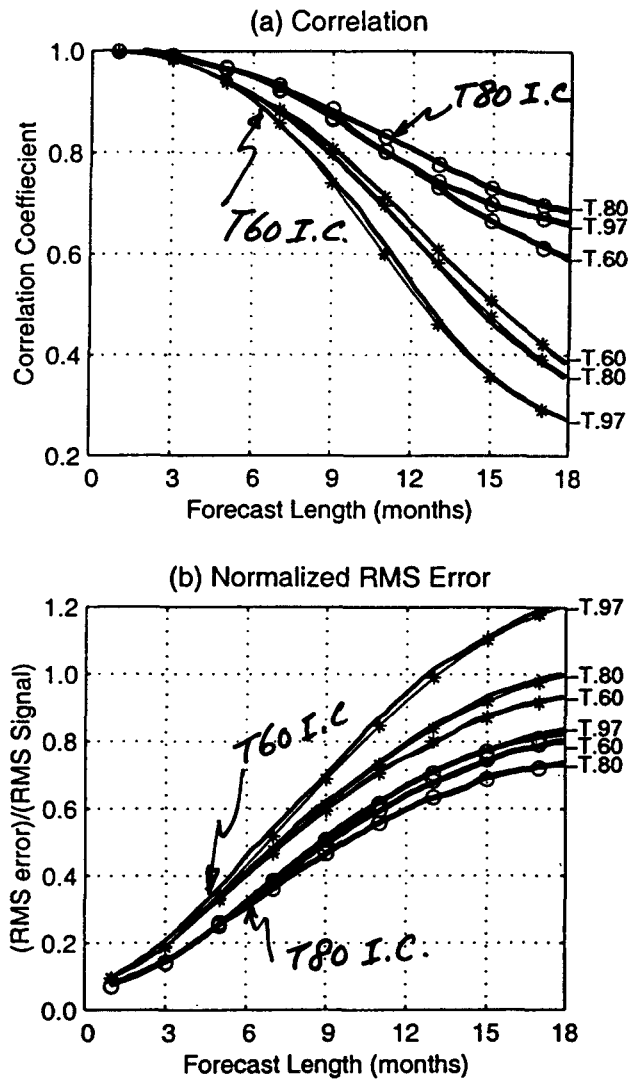
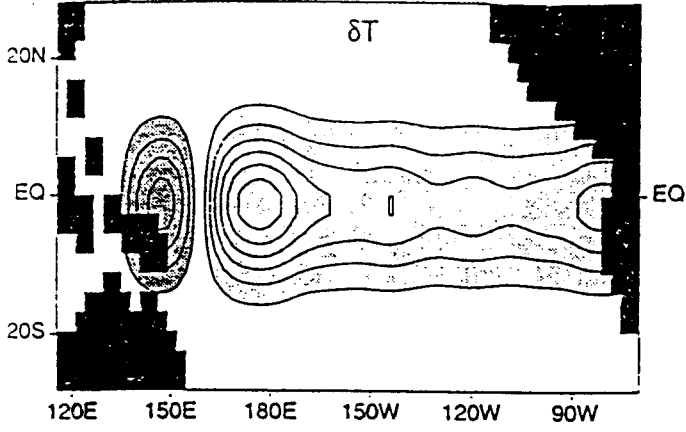
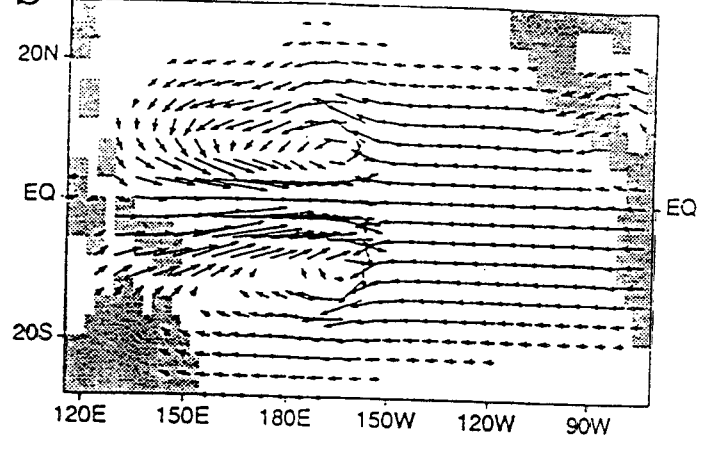


Figure 14. Imperfect Model Predictions. These graphs show the results of using one model to forecast the simulated data produced by a different model. The Nino3 index has been used as the metric to evaluate skill. Panel (a) shows the correlation for forecasts of the T.80 simulated data (circles) using the T.97, T.80 and T.60, models. Perfect initial conditions were used to start the forecasts, and hence the two sources of error are (i) errors due to the inherently unpredictable future noise and (ii) error due to differences between the forecast model and the simulation model. The forecasts are repeated using the T.60 model to simulate the data (curves marked with asterisks). Panel (b) is the same as panel (a) except the RMS error is measured instead of correlation.

a Stochastic Optimal (SST)



b Stochastic Optimal (winds)



c

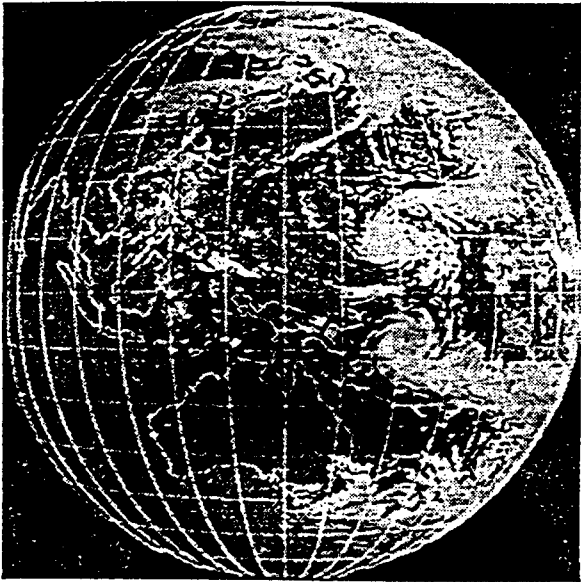


FIG. 7

**Another issue that is not clear at the moment is the nature of the noise. Is there a particular noise structure that ENSO is most sensitive to ? Moore and Kleeman have argued that the intraseasonal oscillation (MJO) is the important noise source of ENSO. However, this issue is far from being settled.**

**The understanding of ENSO irregularity is important because it is directly related to the predictability issue.**

## What Is Known

- ENSO is a coupled phenomenon where the dynamic feedback between trade winds and SST is fundamental.
- ENSO resides in a dynamic regime where the time scales associated with air-sea feedback and oceanic adjustment are comparable. Neither these time scales alone determine the period of ENSO.
- The turnabout between warm and cold phases of ENSO cycle is attributed to subsurface ocean adjustment off the equator.
- Evidence at hand suggests that ENSO is probably weakly nonlinear.
- It is increasingly evident that stochastic processes play an important role in ENSO evolution.

# Unresolved Issues

**What limits ENSO predictability ?**

- Spring predictability barrier
- Stochastic processes
- Decadal modulation of ENSO

**How does ENSO interact with other modes ?**

- Annual cycle  $\Leftrightarrow$  ENSO
- Tropics  $\Leftrightarrow$  extratropics
- Monsoon, TAV  $\Leftrightarrow$  ENSO

**How does global climate change affect ENSO ?**